Unexpected Dispersion-Stabilized Tris(terphenylthiolate) Complexes, $Ln(SAr^{iPr6})_3$, Arising from Two-Electron Reduction by $Ln(SAr^{iPr6})_2$ (Ar^{iPr6} = C_6H_3-2,6-(C_6H_2-2,6,4-$^iPr_3$)$_2$)

Makayla R. Luevano[†], Cary R. Stennett[†], Eric Ma, Joseph W. Ziller, Fillipp Furche*, and William J. Evans*

Department of Chemistry, University of California, Irvine, California, 92697-2025, United States

[†]M.R.L and C.R.S contributed equally to this work.

Supporting Information

The Supporting Information contains:

1. Experimental

General Considerations. All manipulations were performed by using modified Schlenk techniques or in a Vacuum/Atmospheres glovebox under argon. Solvents were degassed by sparging with dry argon before drying and collection using a Grubbs-type[1] solvent purification system (JC Meyer). All physical measurements were recorded under strictly anaerobic and anhydrous conditions. Infrared spectra were recorded on compressed solid samples using an Agilent Cary 630 ATR/FTIR instrument. Electronic spectra were recorded as dilute solutions in the indicated solvent in quartz cuvettes (1 mm path length) using an Agilent Cary 60 UV/vis spectrophotometer. Combustion analyses were recorded using a ThermoScientific FlashSmart CHNS/O Elemental Analyzer at the UC Irvine Materials Research Institute's TEMPR facility in Irvine, California. The instrument was calibrated with five samples of cystine standard of various masses between 1 and 2 mg immediately before use. NMR spectra were recorded using a Bruker AVANCE 600 MHz spectrometer or a Bruker AVANCE 500 MHz spectrometer at 298 K unless otherwise stated and referenced to residual solvent signals. Assignment of the signals of NMR spectra have been provided where possible; but for the paramagnetic complexes, assignments were not possible due to broadening of the signals by the paramagnetism. LaI_3 and NdI_3 were prepared free of donor solvents from the corresponding metal and ammonium iodide using bespoke apparatus made in the UC Irvine Glass Shop as previously described.[2] $KSAr^{iPr6}$ was prepared by the reaction between $HSAr^{iPr6}$ with potassium metal in toluene as previously described.[3] The $Ln(SAr^{iPr6})_2$ complexes, **1-Ln**, were prepared by reduction of $Ln(SAr^{iPr6})_2I$ (prepared from LnI_3[2] and the potassium thiolate[3]) with KC_8 as previously described.[4] $K_2(C_8H_8)$ was prepared by treatment of C_8H_8 with potassium metal in diethyl ether at -35 °C (*CAUTION: $K_2(C_8H_8)$*

explodes upon contact with air and appropriate precautions must be taken during its synthesis, use, and disposal).

Synthesis of La(SAr^{iPr6})(C_8H_8), 2-La, and La(SAr^{iPr6})$_3$, 3-La. In a 20 mL vial, La(SAr^{iPr6})$_2$ (**1-La**, 0.25 g, 0.21 mmol) was dissolved in ca 10 mL of diethyl ether to afford a dark brown solution. 1,3,5,7-cyclooctatetraene (C_8H_8, 0.011 g, 0.11 mmol) was then added in one portion to this stirred solution at ambient temperature. The solution immediately became intense yellow/orange in color and was stirred for 5 min. The solvent was then removed from this solution under reduced pressure to afford an orange residue. The residue was then dissolved in ca. 3 mL of hexane. The vial was sealed and allowed to stand at ambient temperature for 18 h, after which time yellow crystals of La(SAr^{iPr6})(C_8H_8), **2-La**, had formed. The mother liquor was separated from the crystals of **2-La** and transferred to a 20 mL vial. The solvent was removed under reduced pressure. The resulting residue was dissolved in ca. 2 mL of diethyl ether. The vial was then sealed and the solution was allowed to stand at -35 °C. After 18 h, colorless crystals of La(SAr^{iPr6})$_3$, **3-La**, had formed which were suitable for study by X-ray diffraction experiments. Because of the similar solubilities of **2-La** and **3-La**, we were unable to isolate these compounds in pure form by this route. However fractional crystallization of this material permitted the identification of their ^{1}H NMR spectral features. ^{1}H NMR, **3-La** (500 MHz, C_6D_6): δ = 1.14 (d, 12H, J_{HH} = 6.9 Hz, CH(C*H*$_3$)$_2$), 1.28 (d, 12H, J_{HH} = 6.9 Hz, CH(C*H*$_3$)$_2$), 1.39 (d, 12H, J_{HH} = 6.9 Hz, CH(C*H*$_3$)$_2$), 2.80 (sept, 6H, J_{HH} = 6.9 Hz, *p*-C*H*(CH$_3$)$_2$), 3.05 (sept, 12H, J_{HH} = 6.9 Hz, *o*-C*H*(CH$_3$)$_2$), 6.82 (t, 3H, J_{HH} = 7.5 Hz, central ring *p*-C*H*), 6.97 (d, 6H, J_{HH} = 7.5 Hz, central ring *m*-C*H*), 7.24 (s, 12H, flanking ring *m*-C*H*). Minor signals were observed in this spectrum that were consistent with the presence of **2-La** (a singlet resonance at δ = 6.33) and unreacted C_8H_8 (a singlet resonance at δ = 5.64). Combustion analysis

of this material also indicated the presence of minor impurities, but the very high percentages of C and H were in agreement with the high carbon and hydrogen content of **3-La**: Anal. Calcd. for $LaS_3C_{108}H_{149}$: C, 77.2; H, 8.82. Found: C, 79.6; H, 10.68. IR (**3-La**): $\tilde{\nu}$ (cm^{-1}): 2956 (s), 2926 (s, shoulder), 2865 (s), 1605 (m), 1567 (m), 1543 (w), 1459 (s), 1382 (s), 1360 (s), 1337 (w), 1316 (m), 1250 (m), 1189 (w), 1168 (m), 1152 (w), 1108 (m), 1070 (m), 1048 (m), 1003 (w), 939 (m), 921 (m), 813 (m), 874 (s), 848 (w), 819 (w), 796 (s), 775 (m), 743 (s), 730 (s), 696(m), 671 (m). Combustion analysis of the crude solid residue obtained from the reaction between **1-La** and C_8H_8 were consistent with the formation of **2-La** and **3-La**: Anal. Calcd. for $LaS_2C_{152}H_{204}$ (the formula for a 1:1 mixture of **2-La** and **3-La**): C, 74.90; H, 8.44. Found: C, 74.46; H, 8.68.

Synthesis of Nd(SAr^{iPr6})(C_8H_8), 2-Nd, and Nd(SAr^{iPr6})$_3$, 3-Nd. In a manner analogous to the preparation of **2-La** and **3-La**, Nd(SAr^{iPr6})$_2$ (**1-Nd**, 0.20 g, 0.17 mmol) was dissolved in ca 10 mL of diethyl ether in a 20 mL vial to afford a dark brown solution. 1,3,5,7-cyclooctatetraene (C_8H_8, 0.009 g, 0.09 mmol) was then added in one portion to this stirred solution at ambient temperature. The brown color of the solution faded over ca. 10 min and became yellow in color. The solution was then stirred for 4 h. The solvent was then removed from this solution under reduced pressure to afford a green residue. The residue was then dissolved in ca. 3 mL of hexane. The vial was sealed and allowed to stand at -35 °C for 18 h, after which time green/yellow crystals of Nd(SAr^{iPr6})(C_8H_8), **2-Nd**, had formed which were suitable for X-ray diffraction studies. The mother liquor was separated from the crystals of **2-Nd** and transferred to a 20 mL vial. The solvent was removed under reduced pressure. The resulting residue was dissolved in ca. 2 mL of diethyl ether. The vial was then sealed and the solution was allowed to stand at -35 °C. After 18 h, yellow crystals of Nd(SAr^{iPr6})$_3$, **3-Nd**, had formed which were suitable for study by X-ray diffraction

experiments. Because of the similar solubilities of **2-Nd** and **3-Nd**, we were unable to isolate these compounds in pure form by this route. **2-Nd** was therefore prepared by a different route in order to distinguish the spectra of these species (vide infra). The ^{1}H NMR spectrum of the mixture of **2-Nd** and **3-Nd** was compared with that of the separately synthesized **2-Nd** indicated; no signals attributable to paramagnetic **3-Nd** were observed in the region between δ = 100 and -100.

Synthesis of [Nd(SAr^{iPr6})(I)$_2$]$_2$, 4-Nd. NdI_3 (0.47 g, 0.90 mmol) and KSAr^{iPr6} (0.50 g, 0.90 mmol) were combined in ca. 10 mL of diethyl ether in a 20 mL vial to afford a pale blue solution and the mixture was stirred for 18 h. The diethyl ether was then removed from the mixture under reduced pressure to afford a pale blue/green residue. Ca. 10 mL of toluene was added to the residue and the mixture was briefly stirred. The mixture was then centrifuged and the green supernatant was then filtered through a pipette packed with ca. 1 cm of filter paper. The solvent was then removed from the filtrate under reduced pressure to afford a green residue. The residue was triturated 3 times with ca 1 mL portions of hexane. The resulting green residue was again extracted in ca. 5 mL of toluene and the solution was filtered again as above. The green residue was then washed twice with ca. 1 mL portions of hexane and then residual solvent was removed from the green residue to afford 0.23 g (0.26 mmol, 29%)of Nd(SAr^{iPr6})(I)$_2$, **4-Nd**, as a bright green powder. Although combustion analysis of **4-Nd** indicated the presence of minor impurities, this material was successfully used in the synthesis of Nd(SAr^{iPr6})(C_8H_8), **2-Nd** without further purification (vide infra). Anal. Calcd. for $NdSI_2C_{36}H_{49}$: C, 47.42; H, 5.42. Found: C, 45.88; H, 5.26. ^{1}H NMR (500 MHz, C_6D_6): δ = 17.86 ($\Delta\nu_{1/2}$ = 201 Hz), 17.17 ($\Delta\nu_{1/2}$ = 209 Hz), 15.28 ($\Delta\nu_{1/2}$ = 490 Hz), 13.47 ($\Delta\nu_{1/2}$ = 175 Hz), 9.83 ($\Delta\nu_{1/2}$ = 192 Hz), 6.21 ($\Delta\nu_{1/2}$ = 204 Hz), 4.73 ($\Delta\nu_{1/2}$ = 331 Hz), 4.20 ($\Delta\nu_{1/2}$

= 159 Hz), -5.96 ($\Delta\nu_{1/2}$ = 206 Hz), -16.24 ($\Delta\nu_{1/2}$ = 386 Hz), -27.38 ($\Delta\nu_{1/2}$ = 433 Hz). IR: $\tilde{\nu}$ (cm^{-1}): 2955 (s), 2924(m), 2864 (m), 1605 (w), 1567 (w), 1533 (w), 1457 (s), 1407 (w), 1388 (s), 1360(s), 1335 (w), 1316 (m), 1249 (w), 1186 (w), 1167 (w), 1141 (w), 1106 (m), 1068 (w), 1045 (m), 1005 (w)m 956 (w), 926 (w), 921 (w) 897 (s), 872 (s), 847 (w), 820 (w), 799 (s), 774 (w), 747 (s), 725 (s), 695 (w), 681 (w). Crystals of **4-Nd·(toluene)$_2$** which were suitable for study by X-ray diffraction studies were grown from a concentrated solution of **4-Nd** in toluene which was stored at ambient temperature for 18 h.

Synthesis of Nd(SAr^{iPr6})(C_8H_8), 2-Nd, from Nd(SAr^{iPr6})(I)$_2$ and $K_2(C_8H_8)$. Nd(SAr^{iPr6})(I)$_2$ (0.25 g, 0.27 mmol) was dissolved in ca. 7 mL of diethyl ether in a 20 mL vial to give a bright green solution. $K_2(C_8H_8)$ (0.050 g, 0.27 mmol) was then added to this stirred solution in one portion. The solution immediately became yellow/green in color and was allowed to stir for ca. 18 h at room temperature. After, the solvent was removed under reduced pressure and the solid residue was extracted in ca. 10 mL of hexane. The mixture was centrifuged and the yellow supernatant was then filtered through a glass pipette packed with ca. 1 cm of filter paper. The solvent was then removed from the filtrate under reduced pressure. Hexane (ca. 4 mL) was slowly added to the residue with stirring until the residue was almost entirely dissolved. The solution was then filtered again as described above and the filtrate was sealed in a 20 mL vial which was then stored at -35 °C. After 18 h, a large crop of green/yellow crystals of Nd(SAr^{iPr6})(C_8H_8) (**2-Nd**, 0.060 g, 0.080 mmol, 30%) had grown on the walls of the vial. An additional 0.060 g of material was isolated from the mother liquor by repeating the crystallization process described above (overall yield 60%). Anal. Calcd. for $NdSC_{44}H_{57}$: C, 69.33; H, 7.54. Found: C, 68.98; H, 7.63. M.p.: sample changes color from green/yellow to brown from 170-190 °C and melts with decomposition from

195-197 °C. ^{1}H NMR (500 MHz, C_6D_6): δ = 34.48 (s, br, 1H, $\Delta\nu_{1/2}$ = 118 Hz), 19.78 (s, br, 2H, $\Delta\nu_{1/2}$ = 43 Hz), 17.53 (s, br, 1H, $\Delta\nu_{1/2}$ = 18 Hz), 14.53 (s, br, 2H, $\Delta\nu_{1/2}$ = 14 Hz), 10.99 (s, br, 6H, $\Delta\nu_{1/2}$ = 26 Hz), 9.91 (s, br, 1H, $\Delta\nu_{1/2}$ = 17 Hz), 6.90 (s, br, 6H, $\Delta\nu_{1/2}$ = 33 Hz), 6.73 (s, br, 6H, $\Delta\nu_{1/2}$ = 15 Hz), 4.59 (s, br, 6H, $\Delta\nu_{1/2}$ = 17 Hz), 2.74 (s, br, 1H, $\Delta\nu_{1/2}$ = 35 Hz), 2.49 (s, br, 2H, $\Delta\nu_{1/2}$ = 119 Hz), -9.46 (s, br, 6H, $\Delta\nu_{1/2}$ = 17 Hz), -14.91 (s, br, 8H, $\Delta\nu_{1/2}$ = 162 Hz), -25.80 (s, br, 6H, $\Delta\nu_{1/2}$ = 126 Hz), -26.40 (s, br, 2H, $\Delta\nu_{1/2}$ = 135 Hz); an additional signal was detected at δ = 0.89 which is due to a molecule of hexane that is present in the crystal structure of **2-Nd**. The ^{1}H NMR spectrum of **2-Nd** integrates to 56 protons and not the 57 protons expected from the formula. We do not understand why the resonance for one proton is not observed. Signals located at 3.16 and 2.89 ppm and 1.19 – 1.33 ppm are due to a trace impurity of diamagnetic $(KSAr^{iPr6})_2$. UV-vis: λ max /nm (ε/$M^{-1}cm^{-1}$): 296 (17000). IR: $\tilde{\nu}$ (cm^{-1}) = 2956 (m), 2923 (m, shoulder), 2862 (m), 1605 (w), 1586 (w), 1588 (w), 1567 (w), 1538 (w), 1456 (m), 1413 (w), 1385 (m), 1360 (m) ,1315 (m), 1290 (w), 1255 (w), 1237 (w), 1166 (w), 1150 (w), 1112 (w), 1097 (w), 1081 (w), 1070 (w) 1049 (m), 1003 (w), 959 (w), 938 (2), 921 (w), 893 (m), 872 (m), 795 (m), 772 (w), 759 (w), 742 (m), 733 (m), 695 (s).

2. Vibrational Spectra

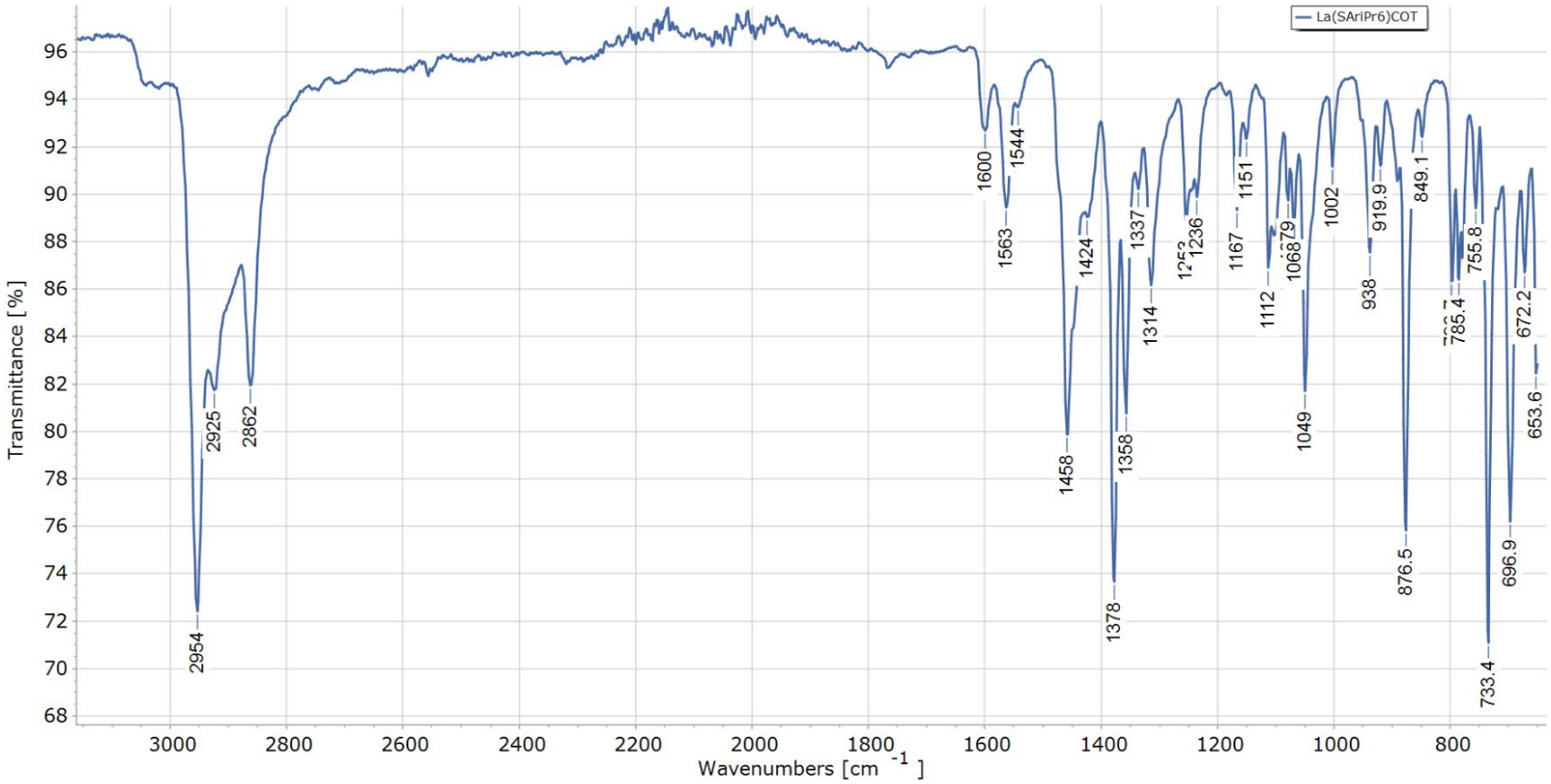

Figure S1. Infrared spectrum of La(SAr^{iPr6})(C_8H_8), **2-La**.

Figure S2. Infrared spectrum of La(SAr^{iPr6})$_3$, **3-La**.

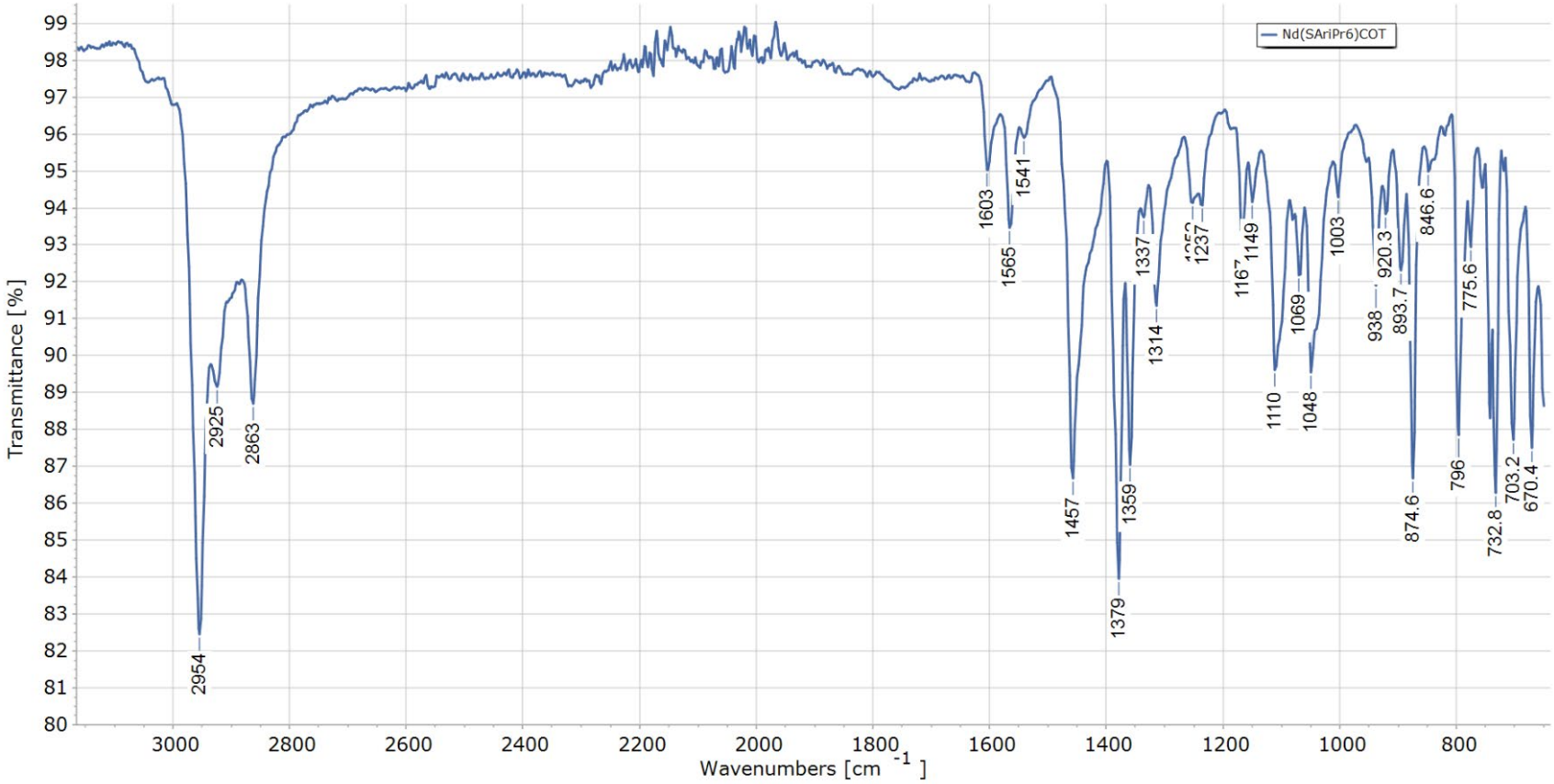

Figure S3. Infrared spectrum of Nd(SAr^{iPr6})(C_8H_8), **2-Nd**, obtained from the reaction between Nd(SAr^{iPr6})$_2$ and C_8H_8.

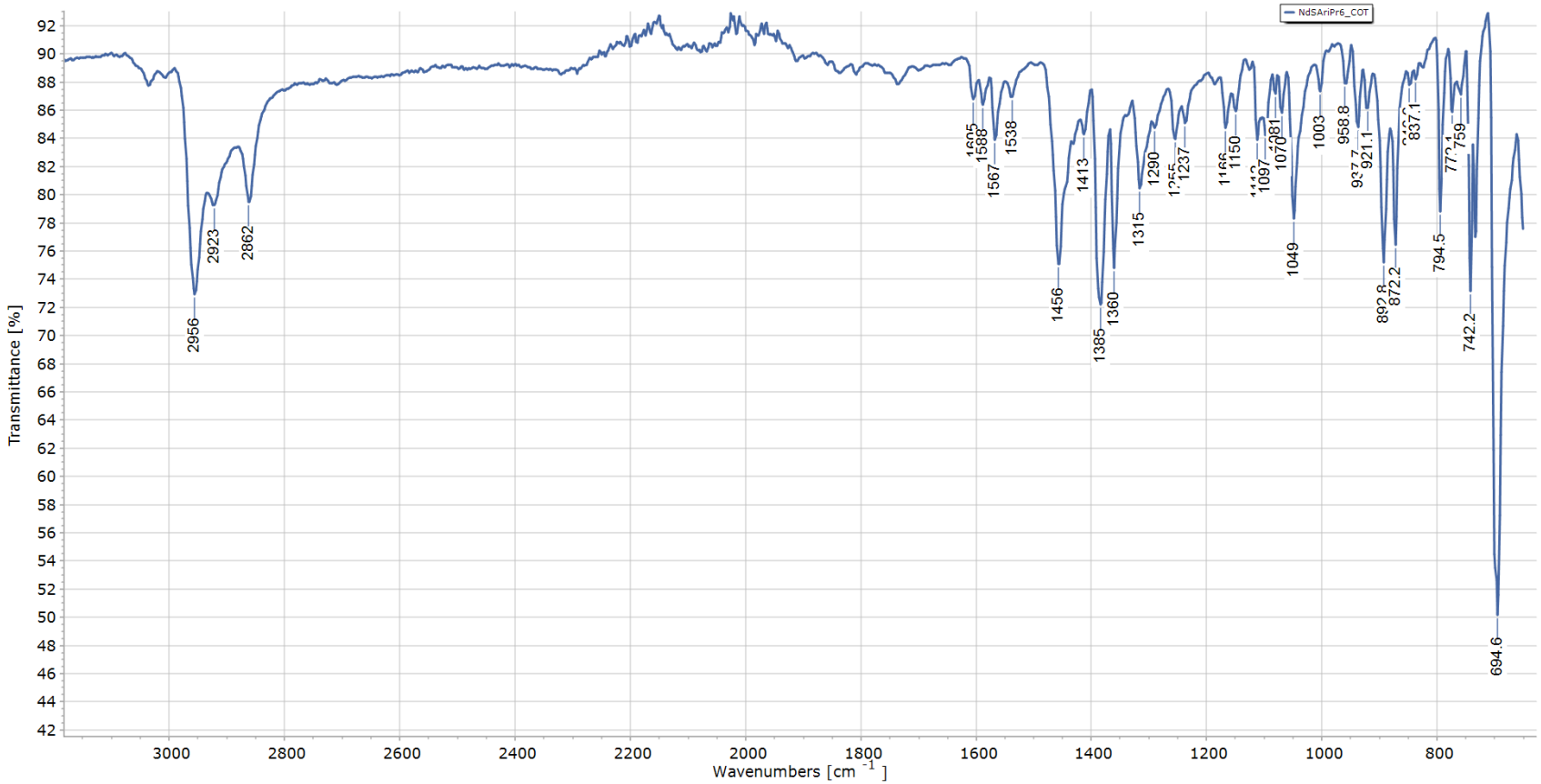

Figure S4. Infrared spectrum of Nd(SAr^{iPr6})(C_8H_8), **2-Nd**, obtained from the reaction between Nd(SAr^{iPr6})$(I)_2$ and $K_2(C_8H_8)$.

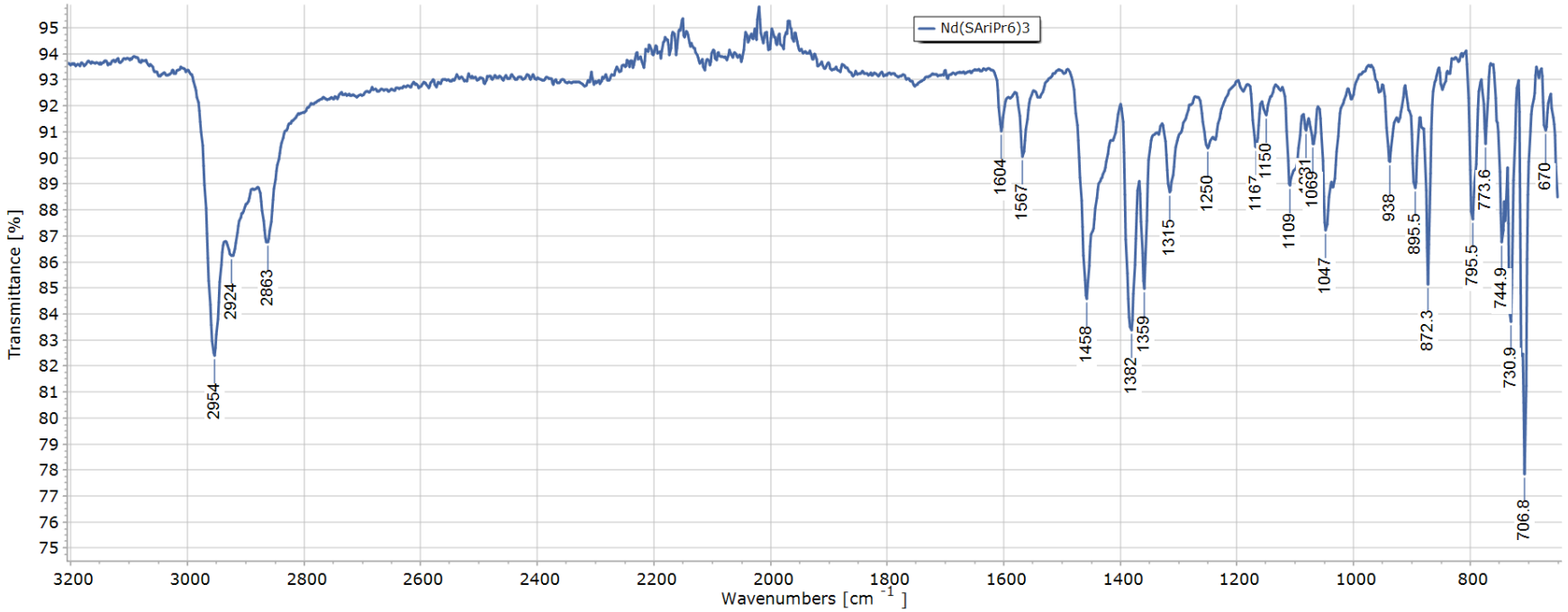

Figure S5. Infrared spectrum of Nd(SAr^{iPr6})$_3$, **3-Nd**.

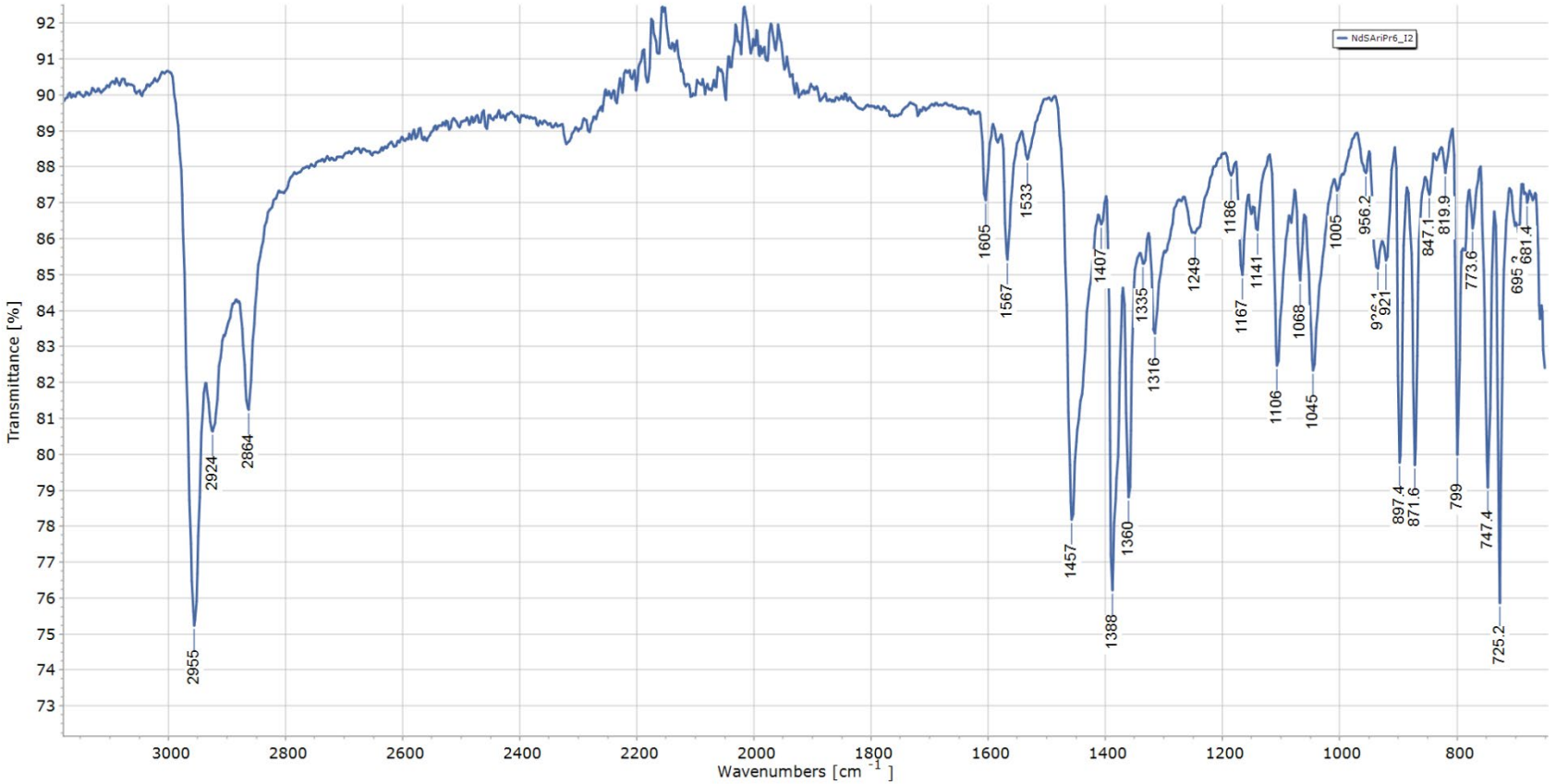

Figure S6. Infrared spectrum of Nd(SAr^{iPr6})(I)$_2$, **4-Nd.**

3. NMR Spectra.

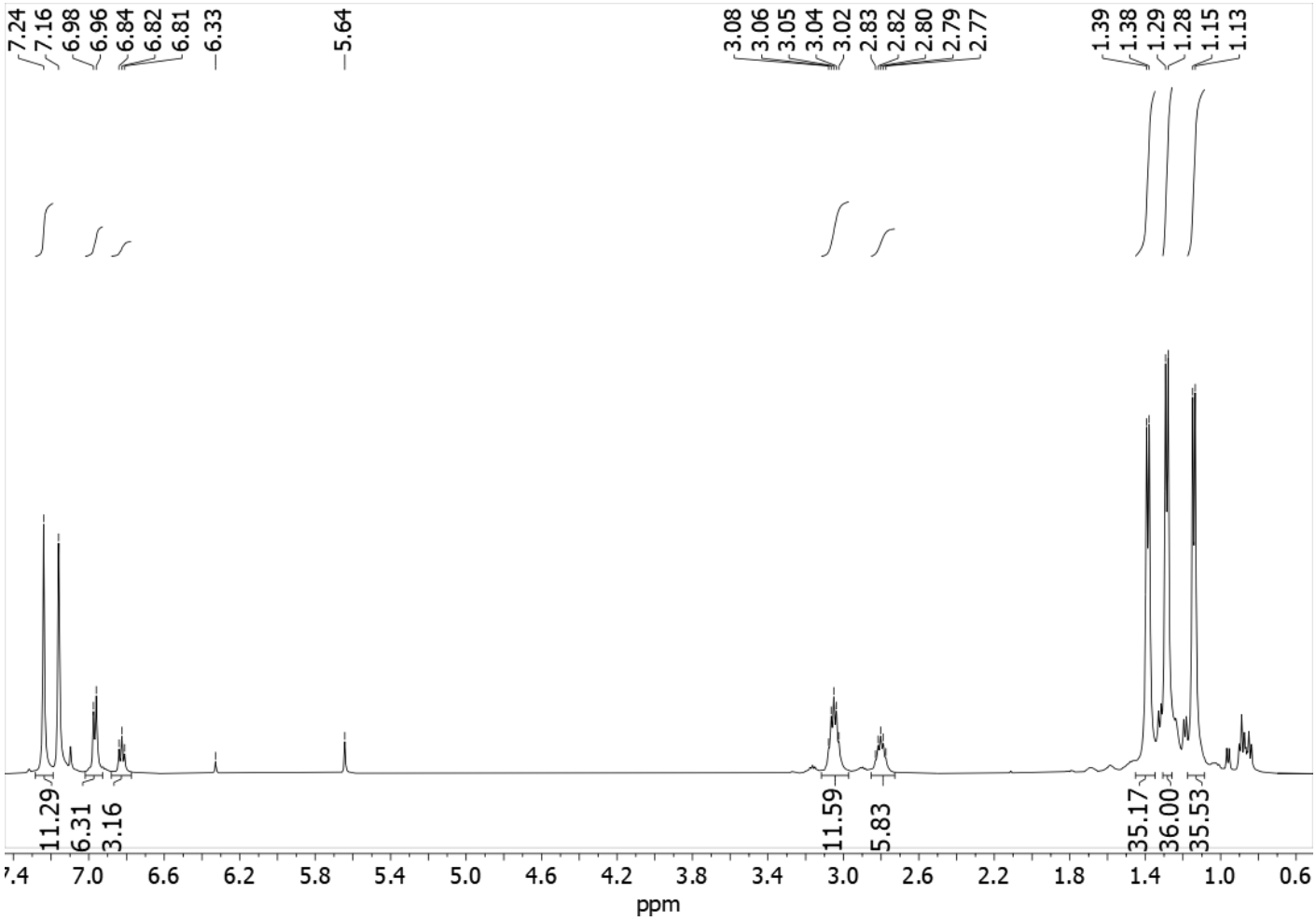

Figure S7. ^{1}H NMR spectrum (500 MHz, C_6D_6) of La(SAr^{iPr6})$_3$, **3-La**. The residual protio signal of the solvent is marked at δ = 7.16, and signals for residual C_8H_8 and La(SAr^{iPr6})(C_8H_8), **2-La**, are found at δ = 5.64 and 6.33, respectively.

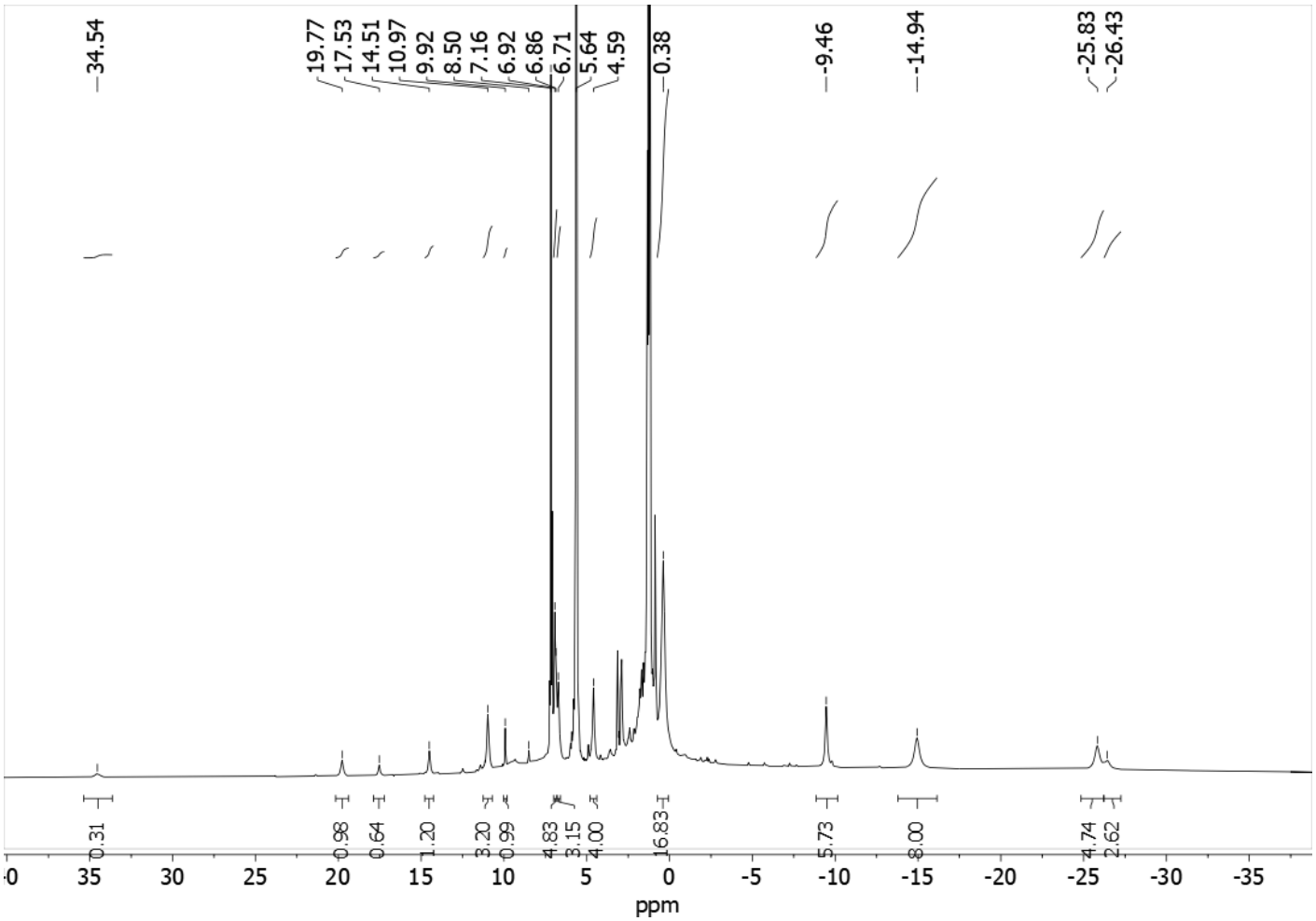

Figure S8. ^{1}H NMR spectrum (500 MHz, C_6D_6) of the crude mixture of Nd(SAr^{iPr6})(C_8H_8), **2-Nd**, and Nd(SAr^{iPr6})$_3$, **3-Nd**, that is formed in the reaction between Nd(SAr^{iPr6})$_2$ and C_8H_8. The residual protio signal of the solvent is marked at δ = 7.16.

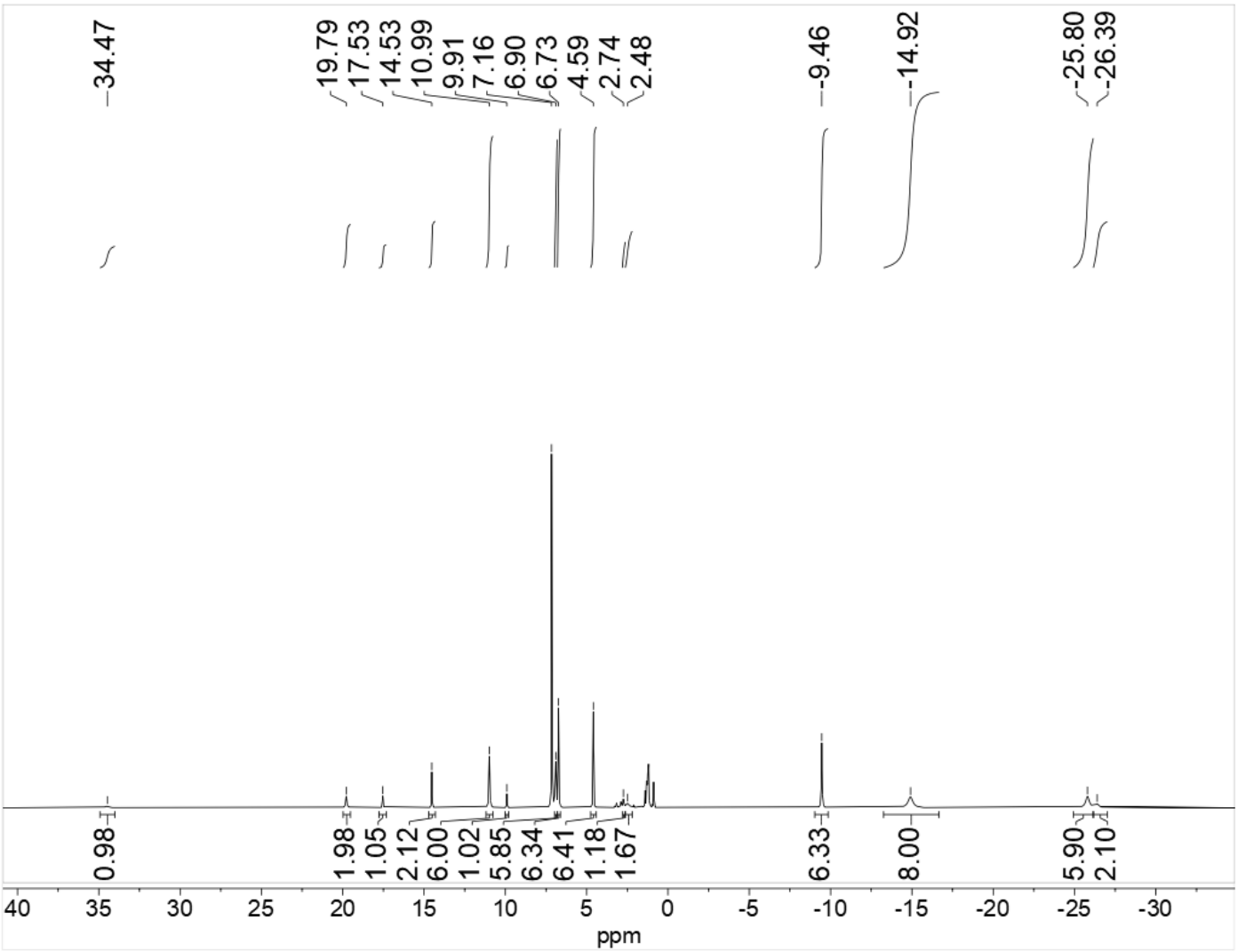

Figure S9. ^{1}H NMR spectrum (500 MHz, C_6D_6) of Nd(SAr^{iPr6})(C_8H_8), **2-Nd**, prepared from the reaction between Nd(SAr^{iPr6})$(I)_2$ and $K_2(C_8H_8)$. The residual protio signal of the solvent is marked at δ = 7.16.

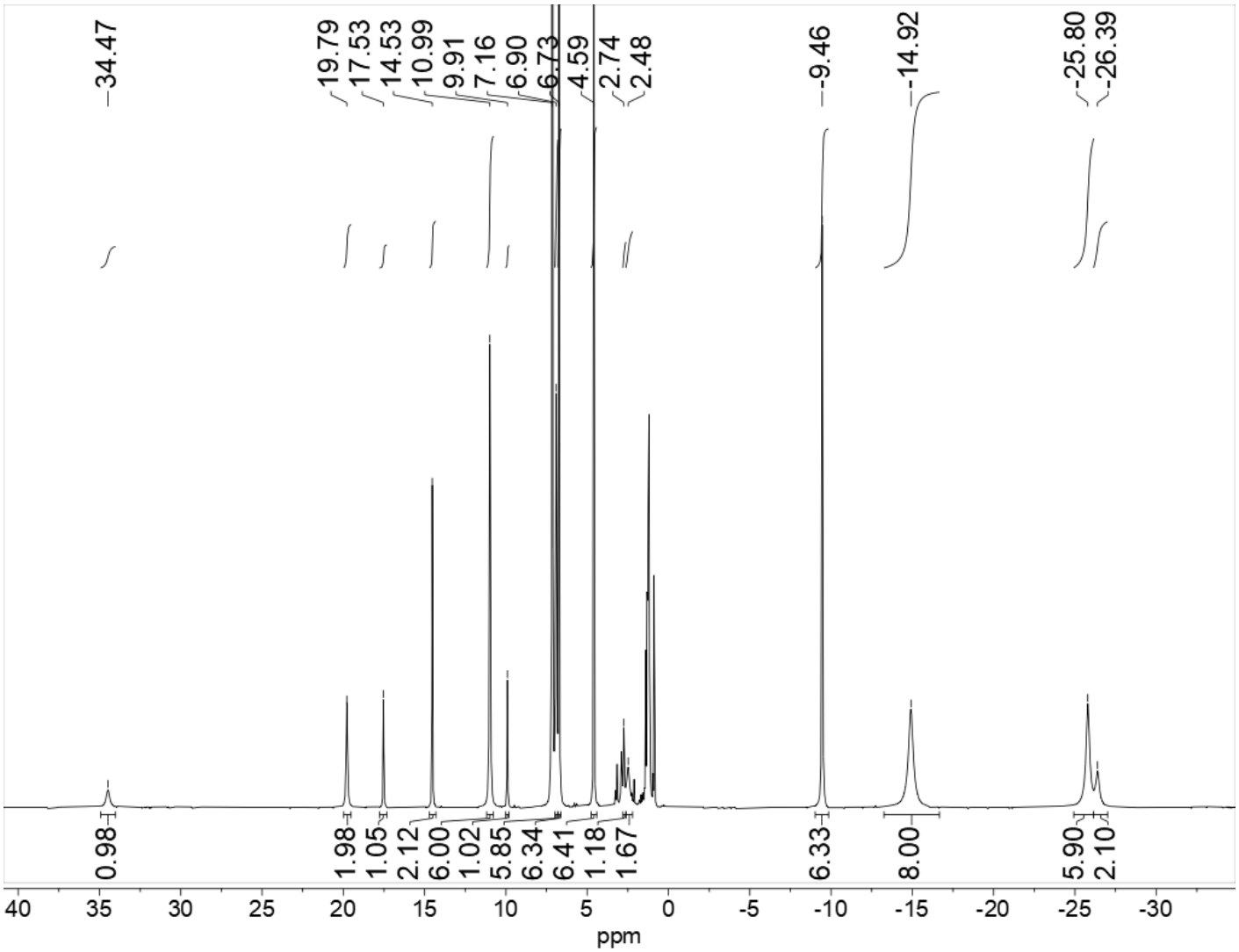

Figure S10. Magnified ^{1}H NMR spectrum (500 MHz, C_6D_6) of Nd(SAr^{iPr6})(C_8H_8), **2-Nd**, prepared from the reaction between Nd(SAr^{iPr6})$(I)_2$ and $K_2(C_8H_8)$. The residual protio signal of the solvent is marked at δ = 7.16.

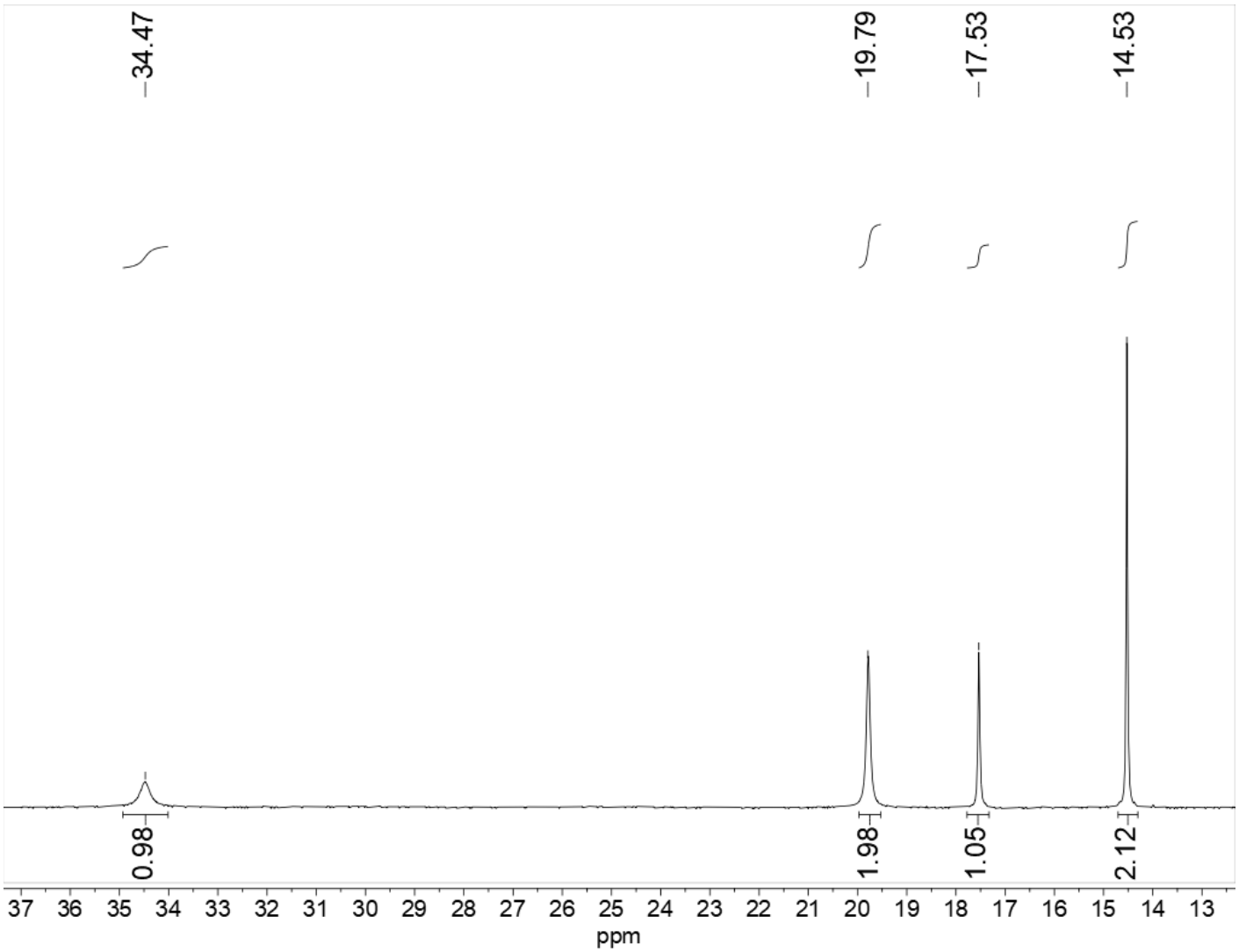

Figure S11. Magnified ^{1}H NMR spectrum (500 MHz, C_6D_6, from δ = 37 to δ = 13) of Nd(SAr^{iPr6})(C_8H_8), **2-Nd**, prepared from the reaction between Nd(SAr^{iPr6})$(I)_2$ and $K_2(C_8H_8)$.

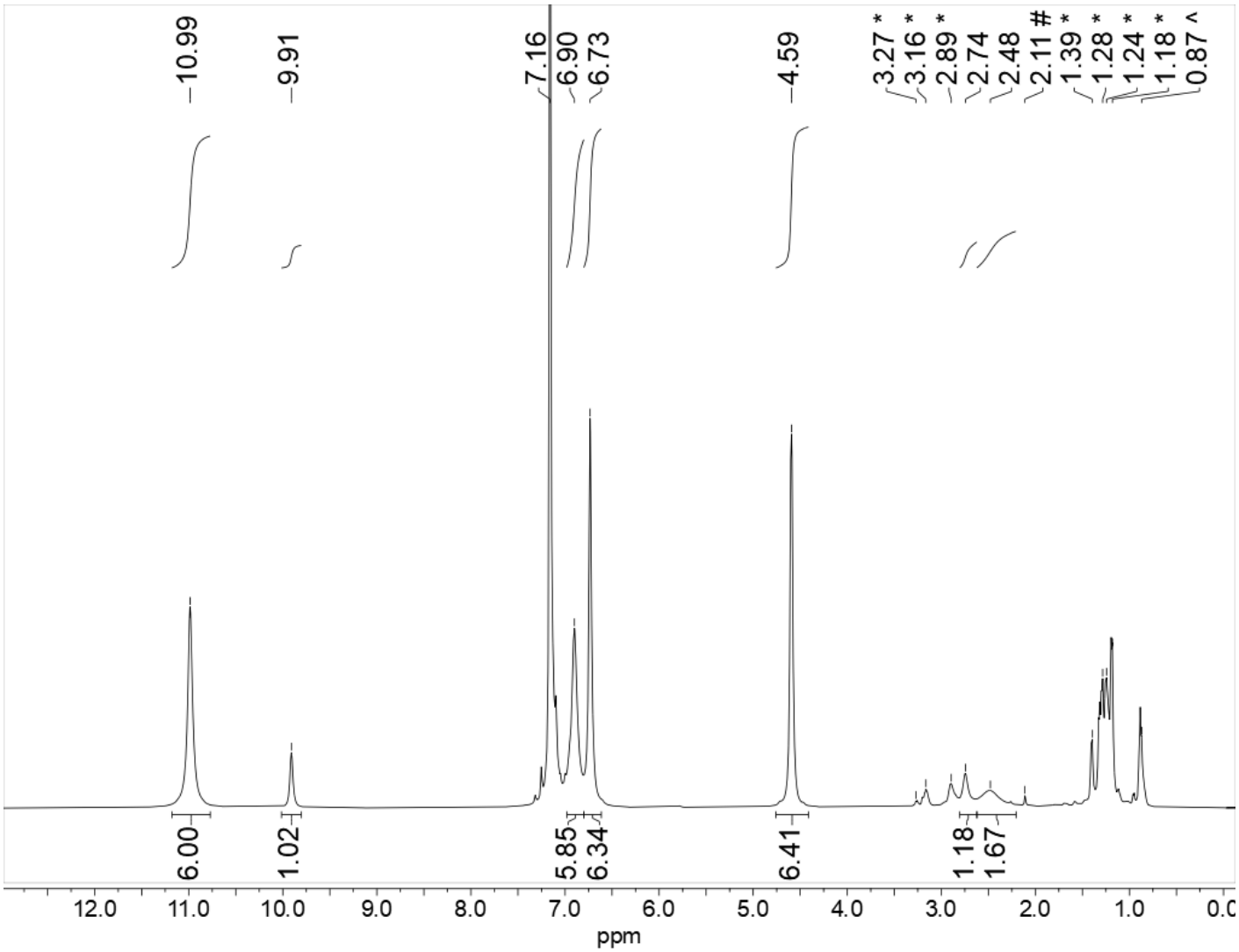

Figure S12. Magnified ^{1}H NMR spectrum (500 MHz, C_6D_6, from δ = 13 to δ = 0) of Nd(SAr^{iPr6})(C_8H_8), **2-Nd**, prepared from the reaction between Nd(SAr^{iPr6})$(I)_2$ and $K_2(C_8H_8)$. The residual protio signal of the solvent is marked at δ = 7.16. The signals marked with "*" correspond to the presence of minor amounts of $(KSAr^{iPr6})_2$ and HSAr^{iPr6}. The signals marked with "#" and "^" correspond to the presence of minor amounts of toluene and hexane, respectively.

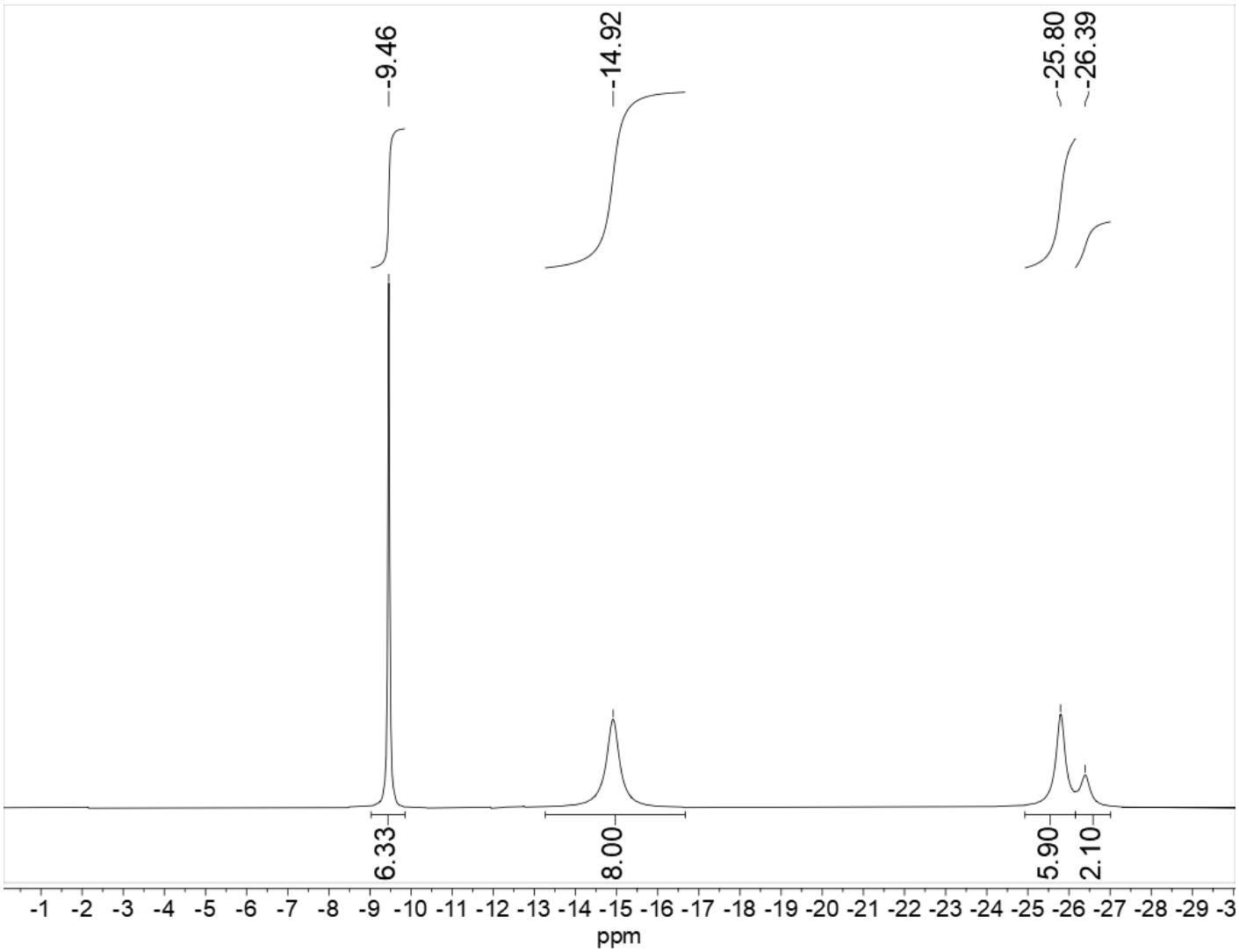

Figure S13. Magnified ^{1}H NMR spectrum (500 MHz, C_6D_6, from δ = 0 to δ = -30) of Nd(SAr^{iPr6})(C_8H_8), **2-Nd**, prepared from the reaction between Nd(SAr^{iPr6})$(I)_2$ and $K_2(C_8H_8)$.

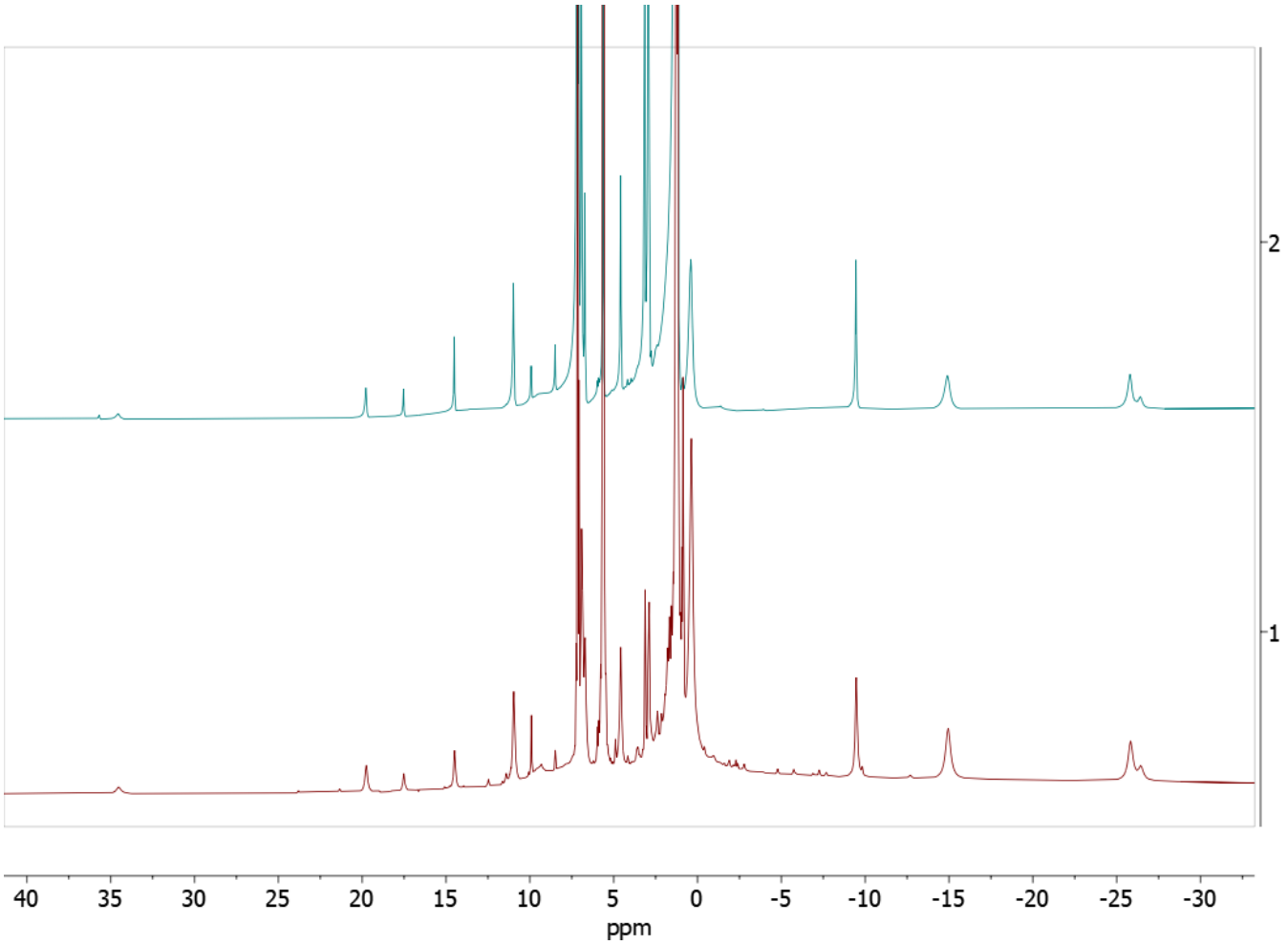

Figure S14. Stacked ^{1}H NMR spectra (500 MHz, C_6D_6) of top: purified Nd(SAr^{iPr6})(C_8H_8), **2-Nd**; and bottom: the crude mixture of Nd(SAr^{iPr6})(C_8H_8), **2-Nd**, and Nd(SAr^{iPr6})$_3$, **3-Nd**, prepared *in situ* by treatment of 100 mg of Nd(SAr^{iPr6})$_2$, **1-Nd**, in 1 mL of C_6D_6 with 1,3,5,7-cyclooctatetraene. The spectra are essentially identical and no resonances attributable to paramagnetic **3-Nd** were found in the region between δ = 100 to -100 ppm. Note: the resonance at δ = 5.64 in both spectra is due to the presence of residual C_8H_8.

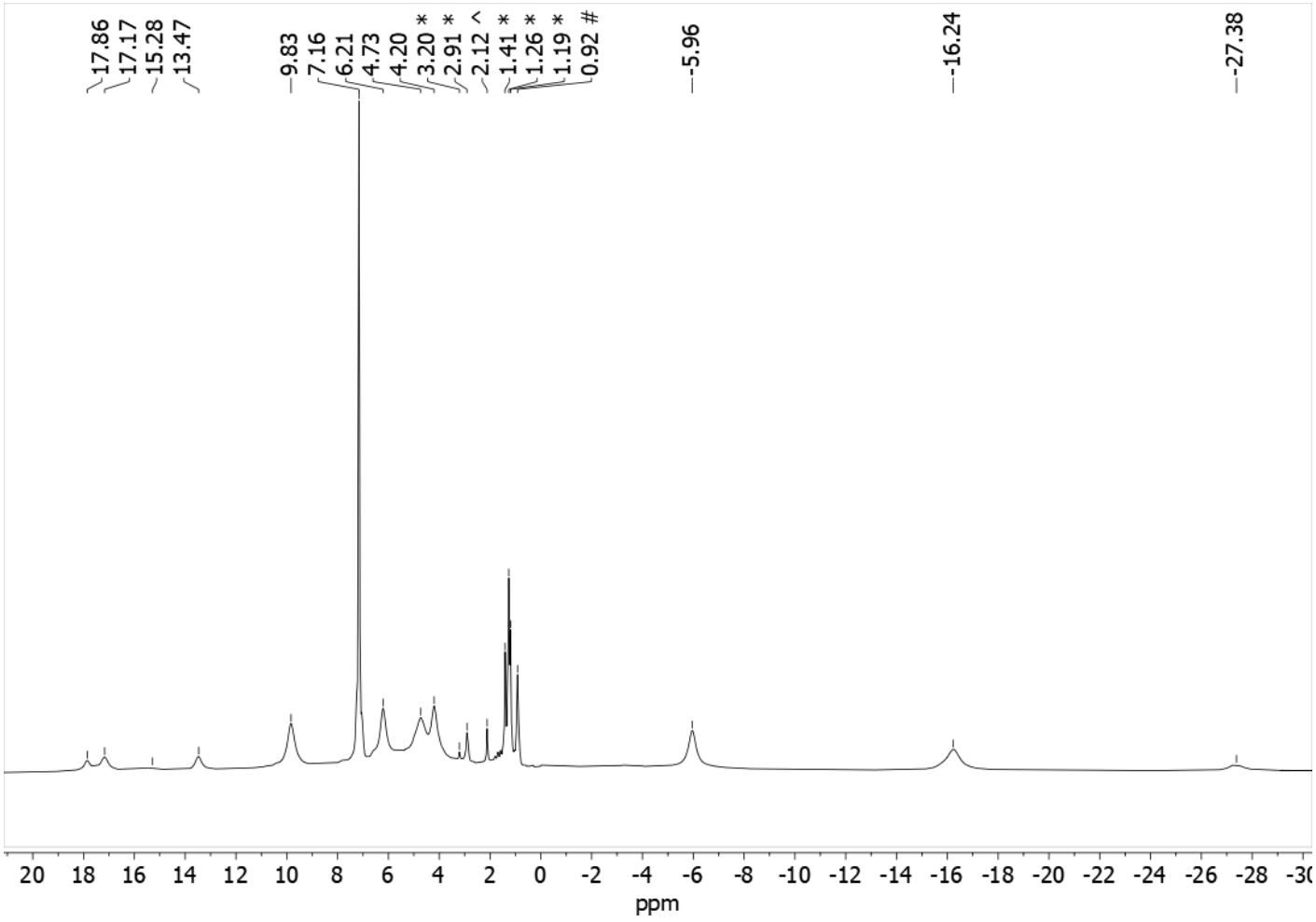

Figure S15. ^{1}H NMR spectrum (500 MHz, C_6D_6) of Nd(SAr^{iPr6})$(I)_2$, **4-Nd**. The residual protio signal of the solvent is marked at δ = 7.16. Minor impurities are marked as follows: * = HSAr^{iPr6}, ^ = toluene, # = hexane.

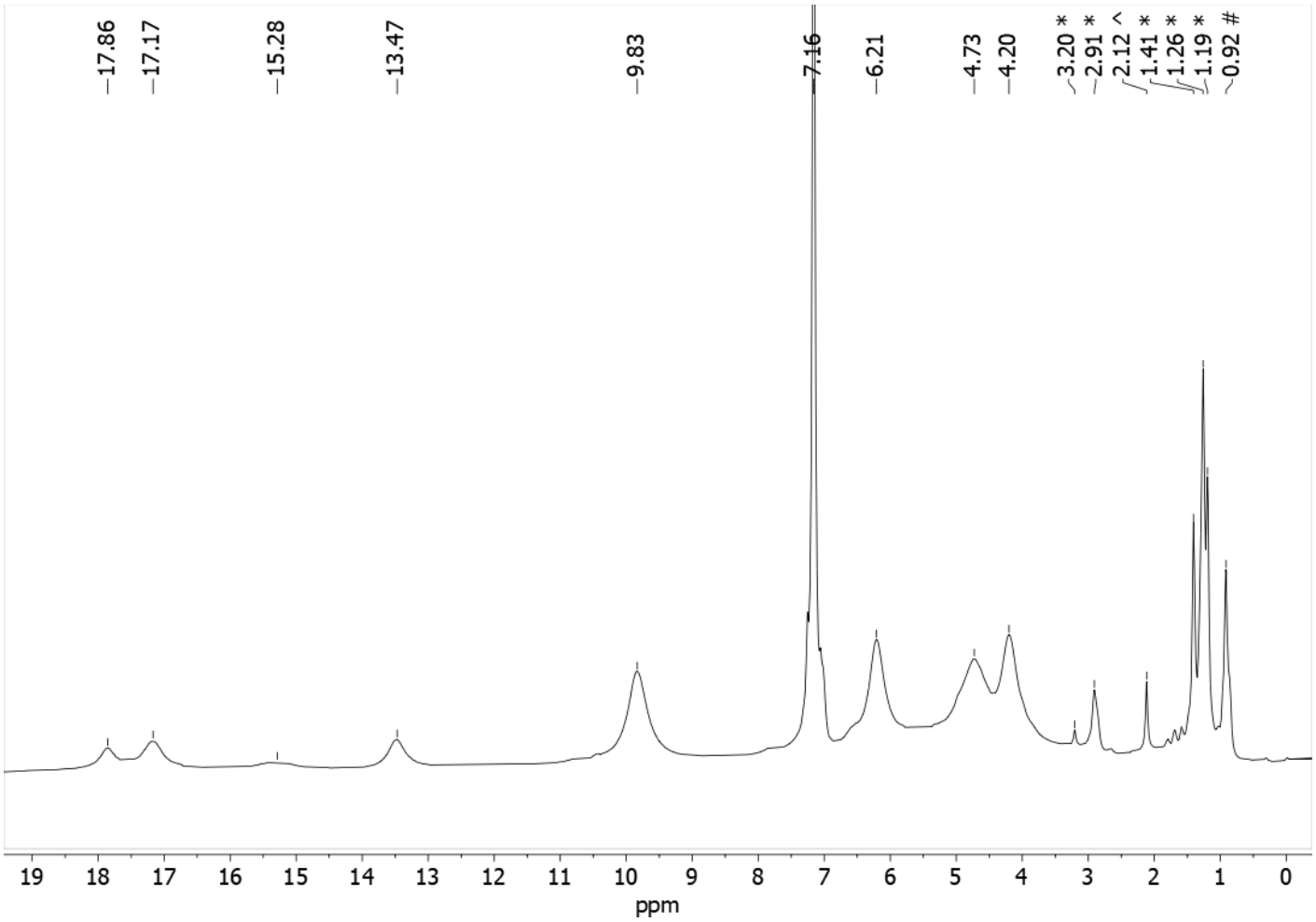

Figure S16. ^{1}H NMR spectrum (500 MHz, C_6D_6, magnified) of Nd(SAr^{iPr6})$(I)_2$, **4-Nd**. The residual protio signal of the solvent is marked at δ = 7.16. Minor impurities are marked as follows: * = HSAr^{iPr6}, ^ = toluene, # = hexane.

4. Electronic Spectra

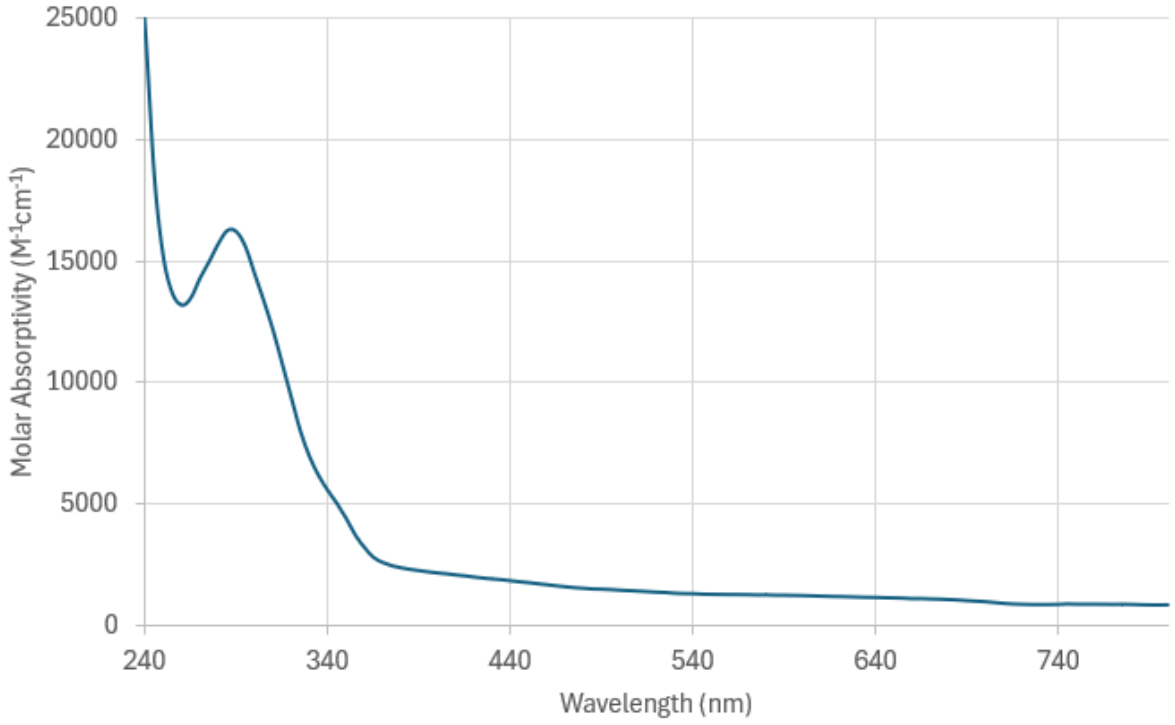

Figure S17. UV-visible spectrum of La(SAr^{iPr6})(C_8H_8), **2-La** (1.3 mM, hexane, 1 mm path length).

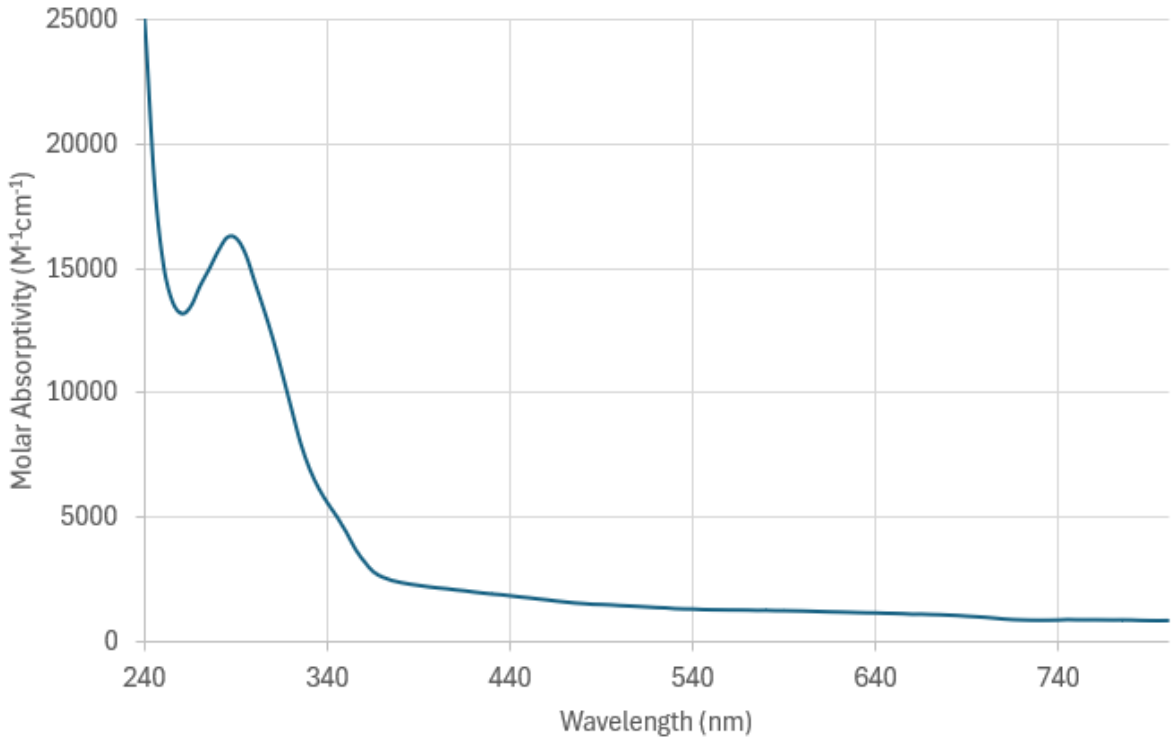

Figure S18. UV-visible spectrum (1.3 mM in hexane, 1 mm path length) of Nd(SAr^{iPr6})(C_8H_8), **2-Nd**, obtained from the reaction between Nd(SAr^{iPr6})$_2$ and C_8H_8.

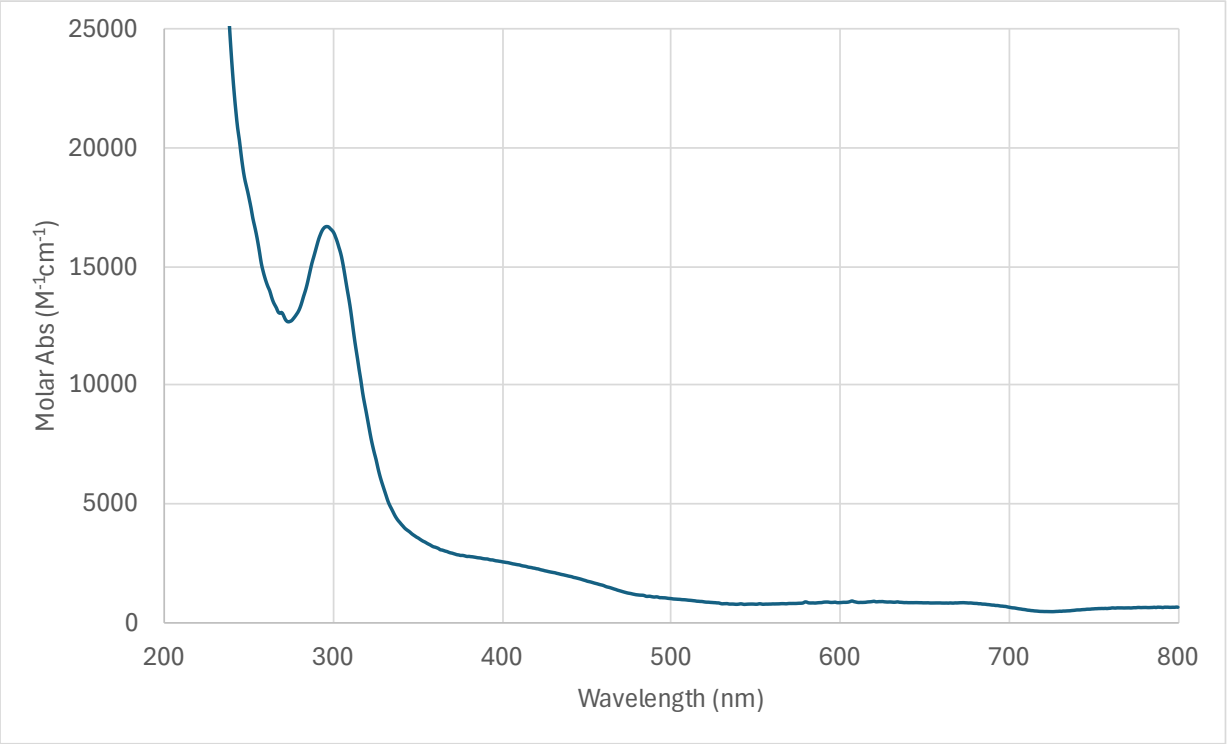

Figure S19. UV-visible spectrum (0.52 mM in hexane, 1 mm path length) of Nd(SAr^{iPr6})(C_8H_8), **2-Nd**, obtained from the reaction between Nd(SAr^{iPr6})$(I)_2$ and $K_2(C_8H_8)$.

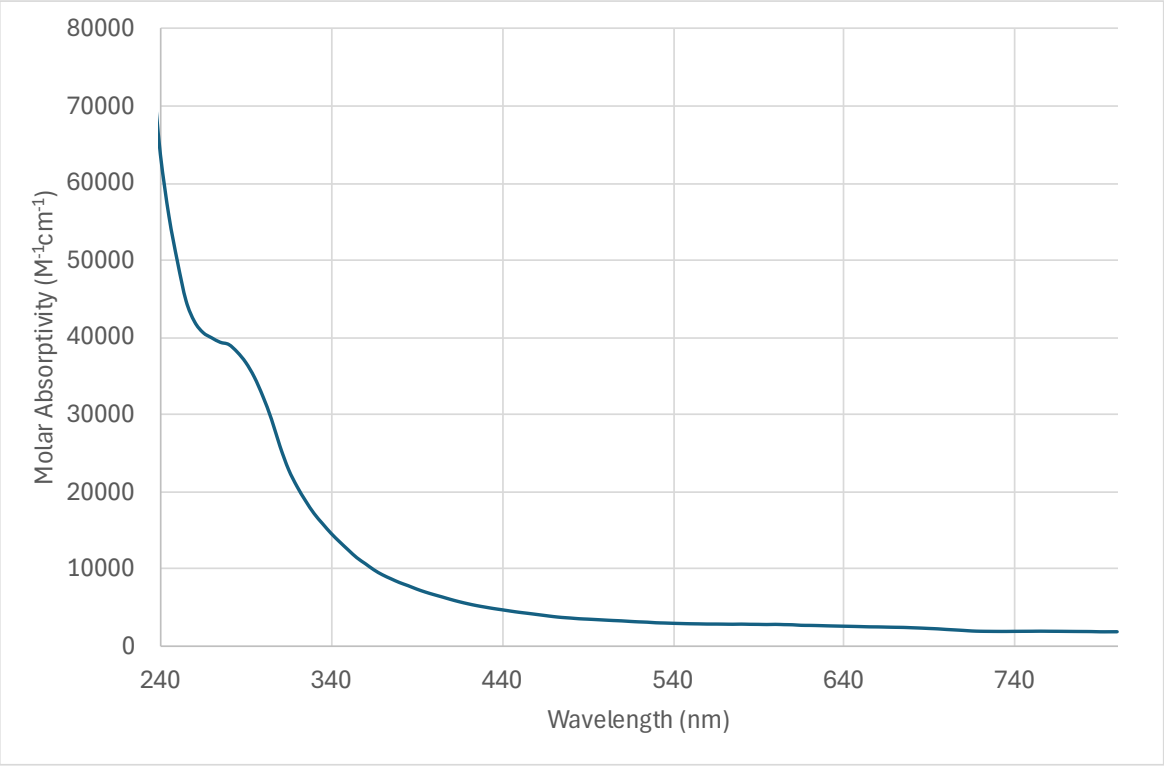

Figure S20. UV-visible spectrum (0.6 mM in hexane, 1 mm path length) of Nd(SAr^{iPr6})$_3$ **3-Nd**, obtained from the reaction between Nd(SAr^{iPr6})$_2$ and C_8H_8.

5. Crystallographic Details.

Table S1. X-ray Data Collection Parameters and Crystallographic Details for La(SAr^{iPr6})(C_8H_8)·C_6H_{14}, **2-La·C_6H_{14}.**

Empirical formula	$C_{50}H_{71}LaS$
Formula weight	843.03
Temperature/K	100.00
Crystal system	monoclinic
Space group	$P2_1/c$
a/Å	16.9455(6)
b/Å	15.7077(5)
c/Å	18.2737(6)
α/°	90
β/°	113.2280(10)
γ/°	90
Volume/Å^3	4469.7(3)
Z	4
ρ_{calc}g/cm^3	1.253
μ/mm^{-1}	1.034
F(000)	1776.0
Crystal size/mm^3	0.125 × 0.065 × 0.054
Radiation	MoKα (λ = 0.71073)
2Θ range for data collection/°	3.55 to 61.014
Index ranges	-24 ≤ h ≤ 24, -21 ≤ k ≤ 22, -25 ≤ l ≤ 26
Reflections collected	87421
Independent reflections	13635 [R_{int} = 0.0649, R_{sigma} = 0.0479]
Data/restraints/parameters	13635/541/720
Goodness-of-fit on F^2	1.009
Final R indexes [I>=2σ (I)]	R_1 = 0.0427, wR_2 = 0.0905
Final R indexes [all data]	R_1 = 0.0739, wR_2 = 0.1030
Largest diff. peak/hole / e Å^{-3}	0.98/-0.68

X-ray Data Collection, Structure Solution and Refinement for La(SAr^{iPr6})(C_8H_8)·C_6H_{14}, 2-La·C_6H_{14}.

A yellow crystal of approximate dimensions 0.054 x 0.065 x 0.125 mm was mounted in a cryoloop and transferred to a Bruker D8 Advance Photon III diffractometer system. The APEX5[5] program package was used to determine the unit-cell parameters and for data collection (30 sec/frame scan time for a sphere of diffraction data). The raw frame data was processed using SAINT[6] and SADABS[7] to yield the reflection data file. Subsequent calculations were carried out using the SHELXTL[8] program package. The diffraction symmetry was 2/*m* and the systematic absences were consistent with the monoclinic space group $P2_1/c$ that was later determined to be correct.

The structure was solved by direct methods and refined on F^2 by full-matrix least-squares techniques. The analytical scattering factors[9] for neutral atoms were used throughout the analysis. Hydrogen atoms were included using a riding model. Disordered atoms were included in the model using multiple components, partial site occupancy factors, and geometric (SADI) and displacement (SIMU) restraints. Least-squares analysis yielded wR2 = 0.1030 and Goof = 1.009 for 720 variables refined against 13635 data (0.70 Å), R1 = 0.0427 for those 9832 data with $I > 2.0\sigma(I)$.

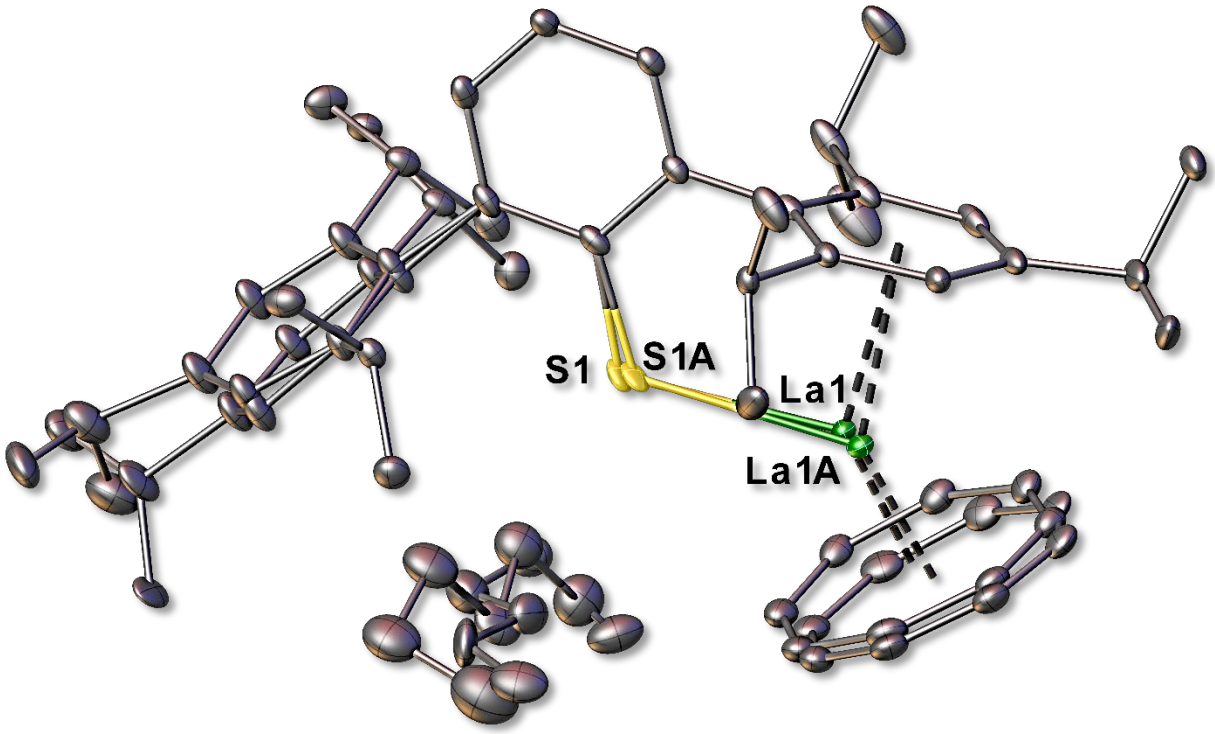

Figure S21. The molecular structure of La(SAr^{iPr6})(C_8H_8), **2-La**, including modeled disorder and solvent of crystallization (hexane). Thermal ellipsoids are drawn at 30% probability. For clarity, hydrogen atoms are not shown.

Table S2. X-ray Data Collection Parameters and Crystallographic Details for La(SAr^{iPr6})(C_8H_8), **2-La.**

Empirical formula	$C_{44}H_{57}LaS$
Formula weight	756.86
Temperature/K	100.00
Crystal system	monoclinic
Space group	$P2_1/c$
a/Å	14.5687(4)
b/Å	17.1846(5)
c/Å	16.8389(5)
α/°	90
β/°	113.6820(10)
γ/°	90
Volume/Å^3	3860.73(19)
Z	4
ρ_{calc}g/cm^3	1.302
μ/mm^{-1}	1.189
F(000)	1576.0
Crystal size/mm^3	0.379 × 0.208 × 0.172
Radiation	MoKα (λ = 0.71073)
2Θ range for data collection/°	3.928 to 66.332
Index ranges	-22 ≤ h ≤ 22, -26 ≤ k ≤ 26, -25 ≤ l ≤ 25
Reflections collected	94116
Independent reflections	14703 [R_{int} = 0.0256, R_{sigma} = 0.0155]
Data/restraints/parameters	14703/0/427
Goodness-of-fit on F^2	1.063
Final R indexes [I>=2σ (I)]	R_1 = 0.0166, wR_2 = 0.0421
Final R indexes [all data]	R_1 = 0.0179, wR_2 = 0.0426
Largest diff. peak/hole / e Å^{-3}	0.52/-0.39

X-ray Data Collection, Structure Solution and Refinement for La(SAr^{iPr6})(C_8H_8), 2-La.

A yellow crystal of approximate dimensions 0.172 x 0.208 x 0.379 mm was mounted in a cryoloop and transferred to a Bruker D8 Advance Photon III diffractometer system. The APEX5[5] program package was used to determine the unit-cell parameters and for data collection (5 sec/frame scan time for a sphere of diffraction data). The raw frame data was processed using SAINT[6] and SADABS[7] to yield the reflection data file. Subsequent calculations were carried out using the SHELXTL[8] program package. The diffraction symmetry was 2/*m* and the systematic absences were consistent with the monoclinic space group $P2_1/c$ that was later determined to be correct.

The structure was solved by direct methods and refined on F^2 by full-matrix least-squares techniques. The analytical scattering factors[9] for neutral atoms were used throughout the analysis. Hydrogen atoms were included using a riding model. Least-squares analysis yielded wR2 = 0.0426 and Goof = 1.063 for 427 variables refined against 14703 data (0.65 Å), R1 = 0.0166 for those 13995 data with $I > 2.0\sigma(I)$.

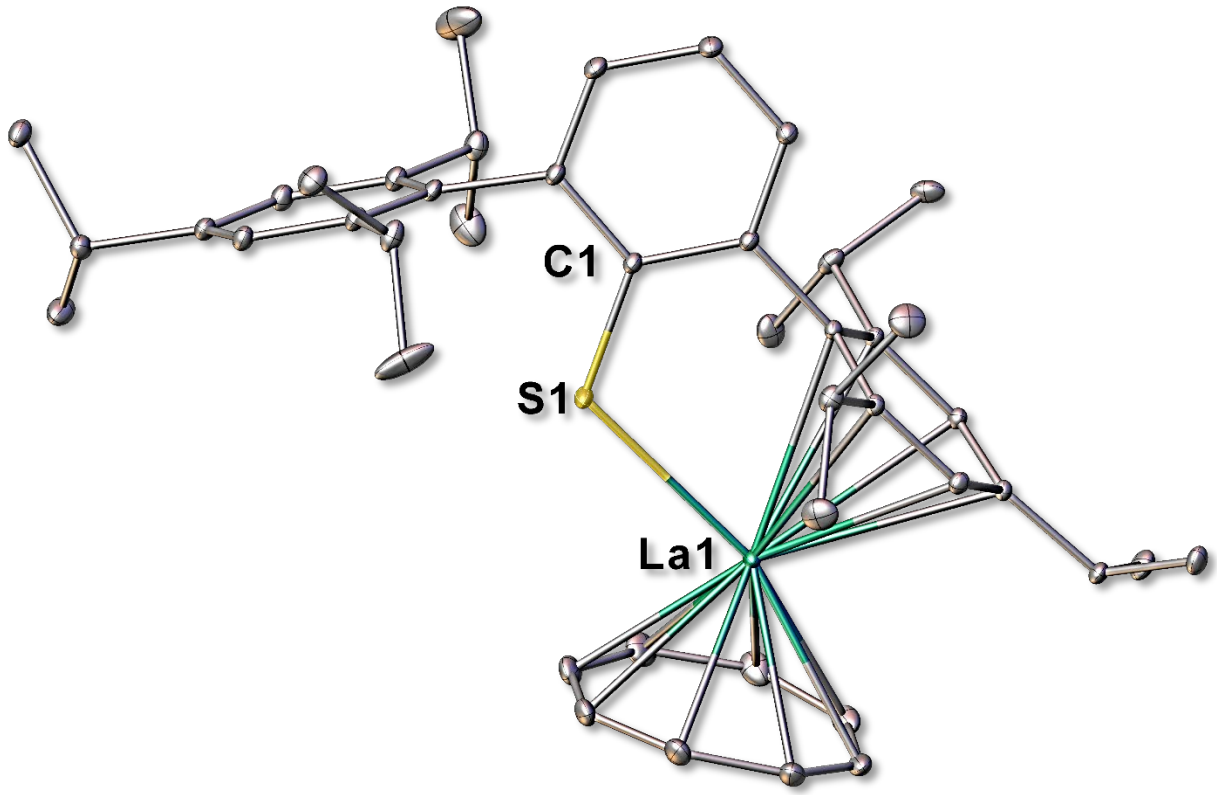

Figure S22. The molecular structure of La(SAr^{iPr6})(C_8H_8), **2-La**, with thermal ellipsoids drawn at 30% probability. For clarity, hydrogen atoms are not shown.

Table S3. X-ray Data Collection Parameters and Crystallographic Details for Nd(SAr^{iPr6})(C_8H_8), **2-Nd.**

Empirical formula	$NdSC_{50}H_{71}$
Formula weight	848.36
Temperature/K	133.15
Crystal system	monoclinic
Space group	$P2_1/c$
a/Å	16.9984(13)
b/Å	15.6051(12)
c/Å	18.0517(14)
α/°	90
β/°	113.5090(10)
γ/°	90
Volume/Å^3	4391.0(6)
Z	4
ρ_{calc}g/cm^3	1.283
μ/mm^{-1}	1.262
F(000)	1788.0
Crystal size/mm^3	0.419 × 0.321 × 0.279
Radiation	MoKα (λ = 0.71073)
2Θ range for data collection/°	2.612 to 61.082
Index ranges	-22 ≤ h ≤ 23, -22 ≤ k ≤ 20, -25 ≤ l ≤ 25
Reflections collected	55043
Independent reflections	13031 [R_{int} = 0.0668, R_{sigma} = 0.0541]
Data/restraints/parameters	13031/30/715
Goodness-of-fit on F^2	1.038
Final R indexes [I>=2σ (I)]	R_1 = 0.0356, wR_2 = 0.0852
Final R indexes [all data]	R_1 = 0.0484, wR_2 = 0.0931
Largest diff. peak/hole / e Å^{-3}	0.97/-1.08

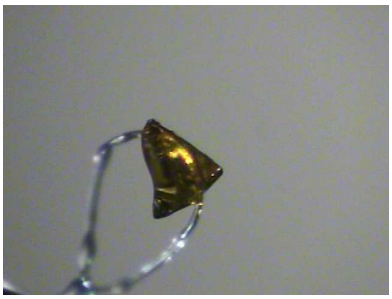

X-ray Data Collection, Structure Solution and Refinement for Nd(SAr^{iPr6})(C_8H_8), 2-Nd.

A yellow/green crystal of approximate dimensions 0.419 x 0.321 x 0.279 mm was mounted in a cryoloop and transferred to a Bruker SMART APEX II diffractometer system. The APEX2[10] program package was used to determine the unit-cell parameters. Data collection used a 10 sec/frame scan time. The raw frame data was processed using SAINT[6] and SADABS[11] to yield the reflection data file. Subsequent calculations were carried out using the SHELXTL[8] program package. The diffraction symmetry was 2/*m* and the systematic absences were consistent with the monoclinic space group $P2_1/c$ that was later determined to be correct.

The structure was solved by direct methods and refined on F^2 by full-matrix least-squares techniques. The analytical scattering factors[9] for neutral atoms were used throughout the analysis. Hydrogen atoms were included using a riding model. Least-squares analysis yielded wR2 = 0.0931 and Goof = 1.038 for 715 variables refined against 13031 data (0.70 Å), R1 = 0.0356 for those 10581 data with $I > 2.0\sigma(I)$.

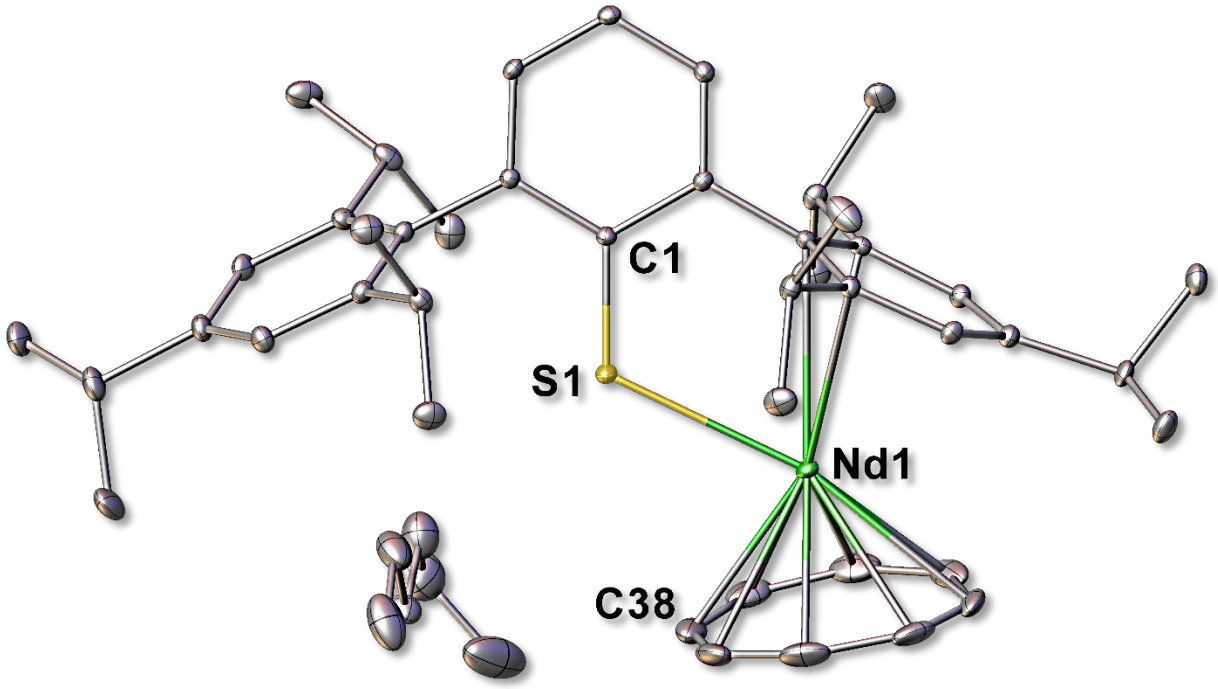

Figure S23. The molecular structure of Nd(SAr^{iPr6})(C_8H_8), **2-Nd**, with thermal ellipsoids drawn at 30%. For clarity, hydrogen atoms are not shown.

Table S4. X-ray Data Collection Parameters and Crystallographic Details for La(SAr^{iPr6})$_3$, **3-La.**

Empirical formula	$C_{108}H_{147}LaS_3$
Formula weight	1680.34
Temperature/K	100.11
Crystal system	monoclinic
Space group	$P2_1/c$
a/Å	14.8533(10)
b/Å	44.125(3)
c/Å	16.4431(11)
α/°	90
β/°	100.2320(10)
γ/°	90
Volume/Å^3	10605.5(13)
Z	4
ρ_{calc}g/cm^3	1.052
μ/mm^{-1}	0.503
F(000)	3600.0
Crystal size/mm^3	0.178 × 0.104 × 0.084
Radiation	MoKα (λ = 0.71073)
2Θ range for data collection/°	3.342 to 61.08
Index ranges	-21 ≤ h ≤ 20, -63 ≤ k ≤ 63, -21 ≤ l ≤ 23
Reflections collected	142360
Independent reflections	32455 [R_{int} = 0.0754, R_{sigma} = 0.0714]
Data/restraints/parameters	32455/54/1431
Goodness-of-fit on F^2	1.020
Final R indexes [I>=2σ (I)]	R_1 = 0.0521, wR_2 = 0.1046
Final R indexes [all data]	R_1 = 0.0820, wR_2 = 0.1136
Largest diff. peak/hole / e Å^{-3}	0.85/-0.95

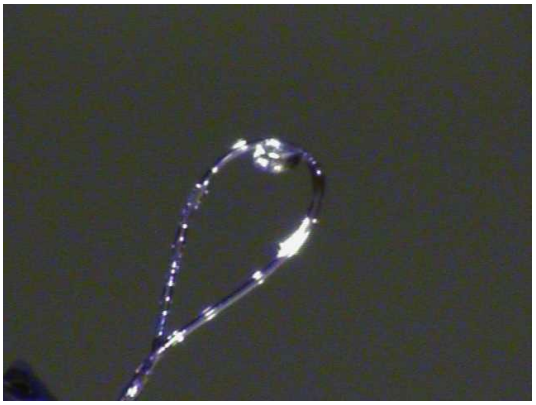

X-ray Data Collection, Structure Solution and Refinement for La(SAr^{iPr6})$_3$, 3-La.

A colorless crystal of approximate dimensions 0.178 x 0.104 x 0.084 mm was mounted in a cryoloop and transferred to a Bruker SMART APEX II diffractometer system. The APEX4[12] program package was used to determine the unit-cell parameters. Data collection used a 60 sec/frame scan time. The raw frame data was processed using SAINT[6] and SADABS[7] to yield the reflection data file. Subsequent calculations were carried out using the SHELXTL[8] program package. The diffraction symmetry was 2/*m* and the systematic absences were consistent with the monoclinic space group $P2_1/c$ that was later determined to be correct.

The structure was solved by direct methods and refined on F^2 by full-matrix least-squares techniques. The analytical scattering factors[9] for neutral atoms were used throughout the analysis. Hydrogen atoms were included using a riding model. Disordered atoms were included in the model using multiple components, partial site occupancy factors, and geometric (SADI, DFIX) and displacement (SIMU) restraints. Least-squares analysis yielded wR2 = 0.1136 and Goof = 1.020 for 1431 variables refined against 32455 data (0.70 Å), R1 = 0.0521 for those 23111 data with $I > 2.0\sigma(I)$.

There were several high residuals present in the final difference-Fourier map. It was not possible to determine the nature of the residuals although it was probable that diethyl ether solvent was present. The SQUEEZE[13] routine in the PLATON[14] program package was used to account for the electrons in the solvent accessible voids.

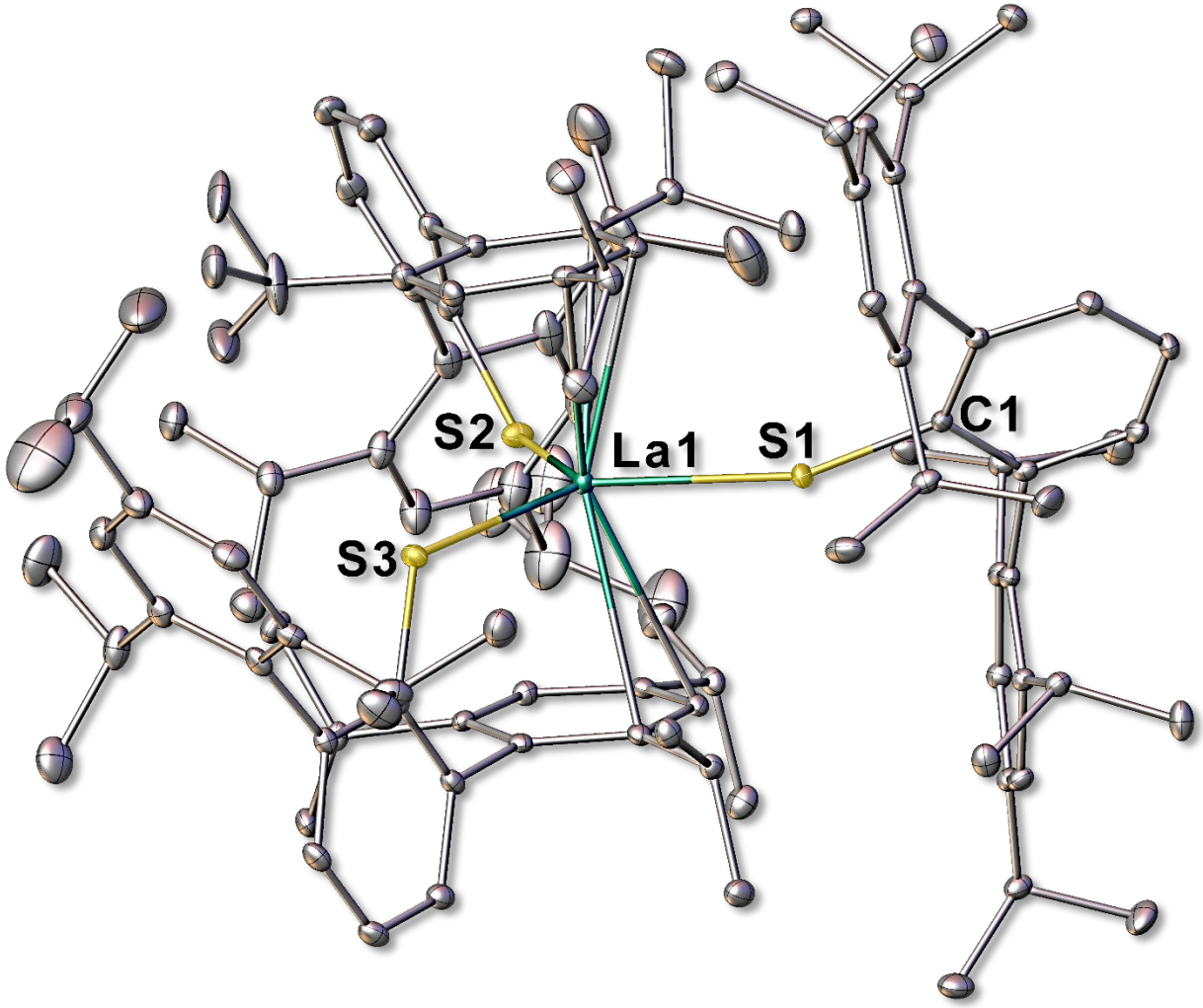

Figure S24. The molecular structure of La(SAr^{iPr6})$_3$, **3-La**, including modeled disorder among the isopropyl substituents, with thermal ellipsoids drawn at 30% probability. For clarity, hydrogen atoms are not shown.

Table S5. X-ray Data Collection Parameters and Crystallographic Details for $Nd(SAr^{iPr6})_3$, **3-Nd.**

Empirical formula	$NdS_3C_{108}H_{147}$
Formula weight	1685.67
Temperature/K	93.15
Crystal system	triclinic
Space group	P-1
a/Å	14.1230(2)
b/Å	18.5883(3)
c/Å	21.7952(3)
α/°	77.9490(10)
β/°	81.4490(10)
γ/°	83.2760(10)
Volume/Å^3	5511.49(14)
Z	2
ρ_{calc}g/cm^3	1.016
μ/mm^{-1}	4.410
F(000)	1806.0
Crystal size/mm^3	0.237 × 0.133 × 0.064
Radiation	CuKα (λ = 1.54178)
2Θ range for data collection/°	4.88 to 144.47
Index ranges	-17 ≤ h ≤ 17, -22 ≤ k ≤ 22, -26 ≤ l ≤ 26
Reflections collected	102450
Independent reflections	20853 [R_{int} = 0.0993, R_{sigma} = 0.0787]
Data/restraints/parameters	20853/108/1133
Goodness-of-fit on F^2	1.052
Final R indexes [I>=2σ (I)]	R_1 = 0.0552, wR_2 = 0.1362
Final R indexes [all data]	R_1 = 0.0734, wR_2 = 0.1458
Largest diff. peak/hole / e Å^{-3}	0.94/-1.45

X-ray Data Collection, Structure Solution and Refinement for Nd(SAr^{iPr6})$_3$, 3-Nd.

A green crystal of approximate dimensions 0.237 x 0.133 x 0.064 mm was mounted in a cryoloop and transferred to a Bruker SMART APEX II diffractometer system. The APEX4[12] program package was used to determine the unit-cell parameters and for data collection (10 to 30 sec/frame scan time). The raw frame data was processed using SAINT[6] and SADABS[7] to yield the reflection data file. Subsequent calculations were carried out using the SHELXTL[8] program package. There were no systematic absences nor any diffraction symmetry other than the Friedel condition. The centrosymmetric triclinic space group $P\bar{1}$ was assigned and later determined to be correct.

The structure was solved by direct methods and refined on F^2 by full-matrix least-squares techniques. The analytical scattering factors[9] for neutral atoms were used throughout the analysis. Hydrogen atoms were included using a riding model. Disordered atoms were included in the model using multiple components and partial site occupancy factors. Least-squares analysis yielded wR2 = 0.1458 and Goof = 1.052 for 1133 variables refined against 20853 data (0.81 Å), R1 = 0.0552 for those 16651 data with I > 2.0σ(I).

There were several high residuals present in the final difference-Fourier map. It was not possible to determine the nature of the residuals although it was probable that diethyl ether solvent was present. The SQUEEZE[13] routine in the PLATON[14] program package was used to account for the electrons in the solvent accessible voids.

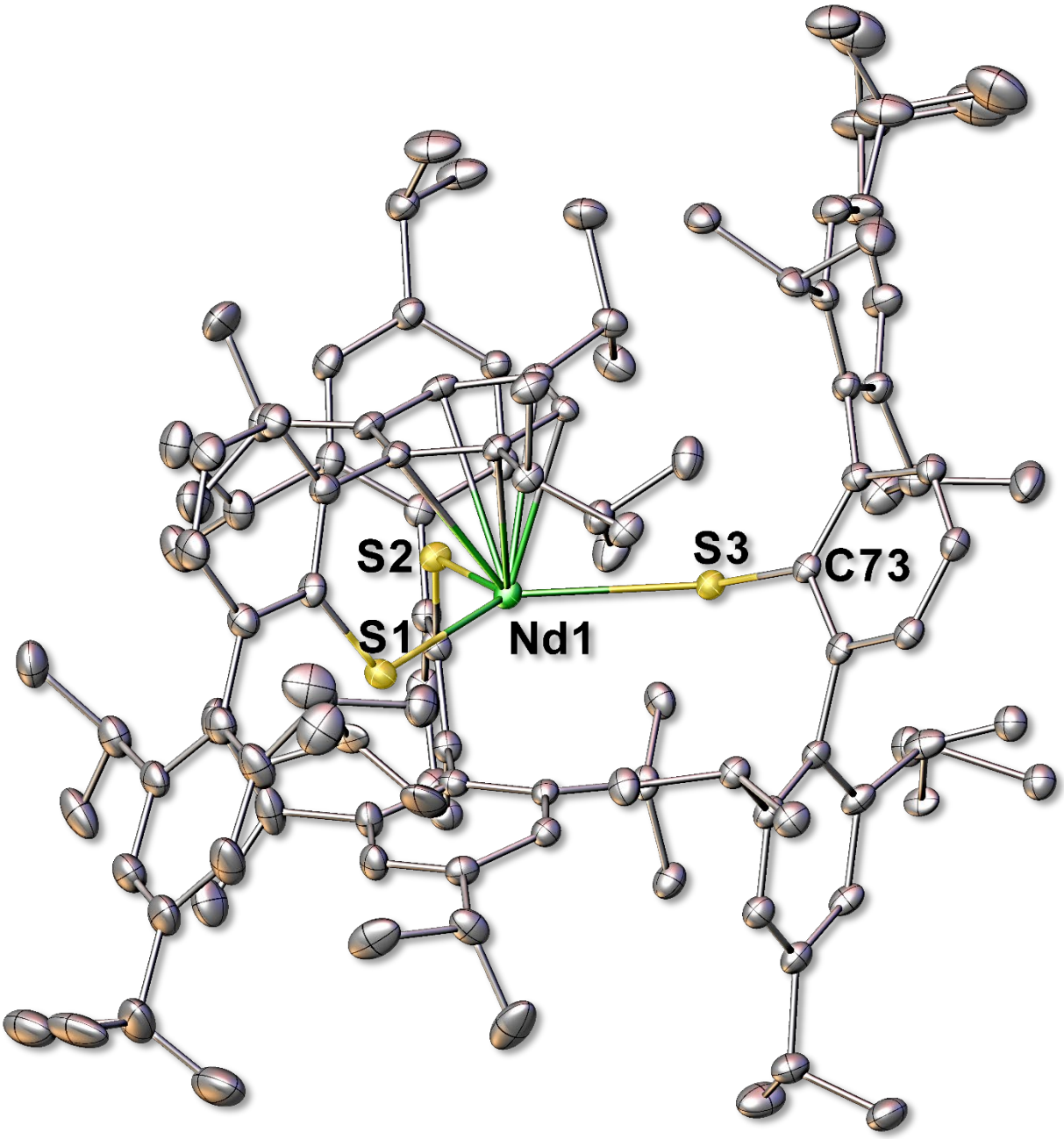

Figure S25. The molecular structure of $Nd(SAr^{iPr6})_3$, **3-Nd**, including modeled disorder among the isopropyl substituents, with thermal ellipsoids drawn at 30% probability. For clarity, hydrogen atoms are not shown.

Table S6. X-ray Data Collection Parameters and Crystallographic Details for $[Nd(SAr^{iPr6})(I)_2]_2$, **4-Nd.**

Empirical formula	$Nd_2S_2C_{86}H_{114}I_4$
Formula weight	2007.97
Temperature/K	93.14
Crystal system	triclinic
Space group	P-1
a/Å	14.301(3)
b/Å	16.545(3)
c/Å	19.403(4)
α/°	75.445(3)
β/°	79.623(3)
γ/°	74.563(3)
Volume/Å^3	4251.9(15)
Z	2
ρ_{calc}g/cm^3	1.568
μ/mm^{-1}	2.749
F(000)	1988.0
Crystal size/mm^3	0.312 × 0.206 × 0.164
Radiation	MoKα (λ = 0.71073)
2Θ range for data collection/°	3.75 to 66.276
Index ranges	-21 ≤ h ≤ 21, -25 ≤ k ≤ 25, -29 ≤ l ≤ 29
Reflections collected	128529
Independent reflections	32098 [R_{int} = 0.0459, R_{sigma} = 0.0438]
Data/restraints/parameters	32098/210/913
Goodness-of-fit on F^2	1.042
Final R indexes [I>=2σ (I)]	R_1 = 0.0284, wR_2 = 0.0543
Final R indexes [all data]	R_1 = 0.0411, wR_2 = 0.0583
Largest diff. peak/hole / e Å^{-3}	0.86/-0.80

X-ray Data Collection, Structure Solution and Refinement for $[Nd(SAr^{iPr6})(I)_2]_2$, 4-Nd.

A green crystal of approximate dimensions 0.164 x 0.206 x 0.312 mm was mounted in a cryoloop and transferred to a Bruker SMART APEX II diffractometer system. The APEX4[12] program package was used to determine the unit-cell parameters and for data collection (10 to 30 sec/frame scan time). The raw frame data was processed using SAINT[6] and SADABS[7] to yield the reflection data file. Subsequent calculations were carried out using the SHELXTL[8] program package. There were no systematic absences nor any diffraction symmetry other than the Friedel condition. The centrosymmetric triclinic space group $P\bar{1}$ was assigned and later determined to be correct.

The structure was solved by direct methods and refined on F^2 by full-matrix least-squares techniques. The analytical scattering factors[9] for neutral atoms were used throughout the analysis. Hydrogen atoms were included using a riding model. Disordered atoms were included in the model using multiple components and partial site occupancy factors. Least-squares analysis yielded wR2 = 0.0582 and Goof = 1.041 for 913 variables refined against 32098 data (0.65 Å), R1 = 0.0284 for those 26060 data with $I > 2.0\sigma(I)$.

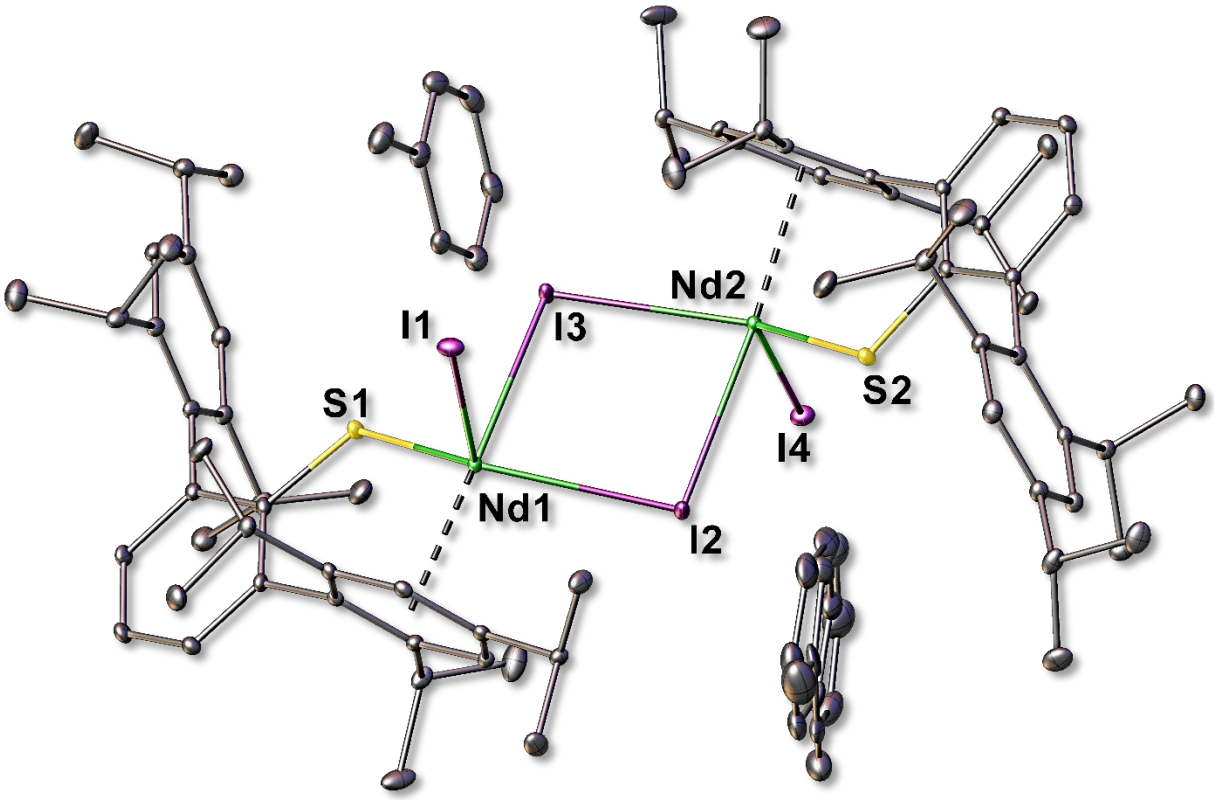

Figure S26. The molecular structure of $[Nd(SAr^{iPr6})(I)_2]_2$, **4-Nd**, including modeled disorder, with thermal ellipsoids drawn at 30% probability. For clarity, hydrogen atoms are not shown.

6. Computational Details.

The TURBOMOLE quantum chemistry software suite (version 7.8)[15] was used for all the calculations. The resolution of identity (RI-J) approximation[16] was used throughout.

Density Functional Theory (DFT) was employed to study the electronic structure of La(SAr^{iPr6})$_3$, **3-La**, and Nd(SAr^{iPr6})$_3$, **3-Nd**. Geometry optimizations were performed on structures obtained from single-crystal X-ray diffraction with hexane solvation effects using the COSMO model,[17] with a dielectric constant of 1.887 and a refractive index of 1.3727. Split-valence basis sets with polarization functions on all non-hydrogen atoms, def2-SV(P),[18] were used for C, H, S atoms, and triple-zeta quality basis sets, def2-TZVP,[19] were used for La and Nd with scalar-relativistic effective core potentials (46 core electrons for La and 28 core electrons for Nd, def2-ecp[20]). The TPSSh[21] functional with D4 dispersion corrections[22] was used to optimize the structures in the solution phase. Singlet and triplet instability analyses[23] were also performed for closed shell singlet states. A numerical quadrature grid[24] of size 4 and weight derivatives were used for exchange-correlation integrals. Ground state energies were converged with a threshold of 10^{-7} a.u. and the Cartesian energy gradient had a maximum norm of 10^{-4} a.u. Kohn-Sham orbitals corresponding to different spin states of each structure. Local minima on the potential energy surface were confirmed by numerical force constant calculations.[25] The VMD program[26] was used to visualize molecular orbitals with a contour value of 0.03. The intramolecular basis set superposition errors (BSSE) were calculated from X-ray structures using the counterpoise method.[27] Bare Fragment calculations were performed by including the charge basis functions

only on atoms in the bare fragment to prevent inconsistencies stemming from the solvation model.

Results. **3-La** and its two constituent fragments underwent geometry optimizations. The fragments were La(SAr^{iPr6})$_2$, comprised of the two "flanking" ligands and La, and the remaining terphenylthiolate, the "terminal" ligand, referred to as "metal" and "ligand" fragments respectively. The metal and ligand fragments were optimized with +1 and -1 charges respectively. The optimized structures were verified to be local minima. No singlet or triplet instabilities were found for **3-La** or its fragments. **Table S7** lists notable bond distances and angles for the crystal structure and the geometry optimized structure for **3-La**.

Table S7. Selected structural parameters (bond distances (Å) and angles (°)) from computed (singlet) structure and crystal structure for La(SAr^{iPr6})$_3$, **3-La**, from DFT calculations using TPSSh, def2-TZVP basis set for La, and def2-SV(P) basis sets for C, H, S.

	Singlet	X-ray
La(1)-S(1) (Å)	2.84	2.8784(6)
La(1)-S(2) (Å)	2.86	2.8310(7)
La(1)-S(3) (Å)	2.82	2.8361(7)
La(1)-Cnt(1) (Å)	2.86	2.802(1)
La(1)-Cnt(2) (Å)	2.93	2.949(1)
S(1)-La(1)-S(2) (°)	134.0	130.40(2)
S(1)-La(1)-S(3) (°)	103.6	112.09(2)
S(2)-La(1)-S(3) (°)	122.4	117.48(2)
Cnt(1)-La(1)-Cnt(2) (°)	161.6	162.15(3)

3-Nd and its two constituent fragments underwent geometry optimizations. The fragments were chosen in the same fashion as **3-La** and optimized with the same charges. The

optimized structures were verified to be local minima. No singlet or triplet instability was found for the ligand fragment. **3-Nd** and the metal fragment were optimized for doublet and quartet states, with the relative ground state energies shown in **Table S8**. **Table S9** lists notable bond distances and angles for the crystal structure and the geometry optimized structure for **3-Nd**.

Table S8. Relative ground state energies for doublet and quartet states of $Nd(SAr^{iPr6})_3$, **3-Nd**, and its constituent metal fragment in reference to the lowest energy state.

Spin State	Relative Full Energy (kcal/mol)	Relative Metal Energy (kcal/mol)
Doublet	30.1	17.4
Quartet	0	0

Table S9. Selected structural parameters (bond distances (Å) and angles (°)) from computed (singlet) structure and crystal structure for $Nd(SAr^{iPr6})_3$, **3-Nd**, from DFT calculations using TPSSh, def2-TZVP basis set for Nd, and def2-SV(P) basis sets for C, H, S.

	Doublet	Quartet	X-ray
Nd(1)-S(1) (Å)	2.77	2.78	2.780(1)
Nd(1)-S(2) (Å)	2.72	2.73	2.7404(9)
Nd(1)-S(3) (Å)	2.78	2.78	2.791(1)
Nd(1)-Cnt(1) (Å)	2.78	2.78	2.61(2)
Nd(1)-Cnt(2) (Å)	2.92	2.92	3.36(2)
S(1)-Nd(1)-S(2) (°)	105.9	107.2	109.97(3)
S(1)-Nd(1)-S(3) (°)	132.6	132.9	130.57(3)
S(2)-Nd(1)-S(3) (°)	121.5	119.9	117.74(3)
Cnt(1)-Nd(1)-Cnt(2) (°)	163.5	163.6	156.06(4)

The two highest occupied molecular orbitals (HOMOs) and the lowest occupied molecular orbital (LUMO) of the entire **3-La** complex were visualized and shown in **Figure S27**. The 3 HOMOs

and the LUMO of the entire **3-Nd** complex in the quartet state were visualized and shown in **Table S10**.

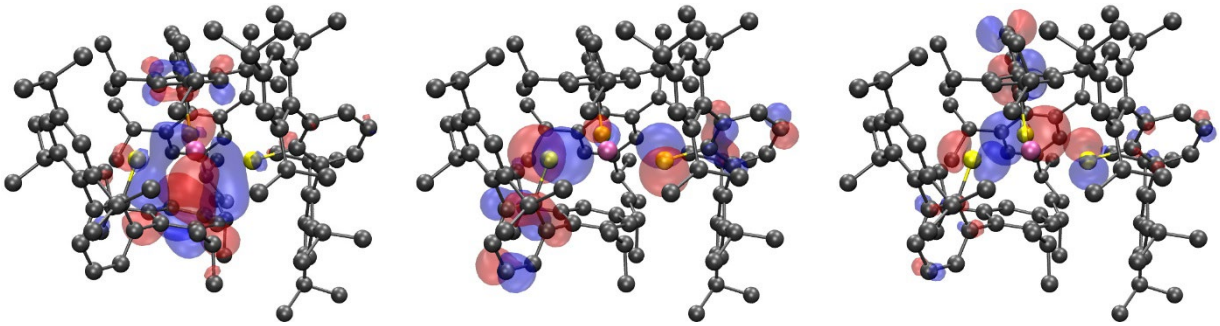

428a (-1.525 eV) 427a (-4.974 eV) 426a (-5.044 eV)

Figure S27. LUMO (left), HOMO (middle) and HOMO-1 (right) (iso 0.03) of La(SAr^{iPr6})$_3$, **3-La**, for singlet state. Hydrogen atoms are omitted for clarity.

Table S10. Visualized molecular orbitals and corresponding energies for the quartet state of Nd(SAr^{iPr6})$_3$, **3-Nd**, at a contour value of 0.03. Hydrogen atoms are omitted for clarity.

Molecular Orbital		Energy (eV)
LUMO (α)	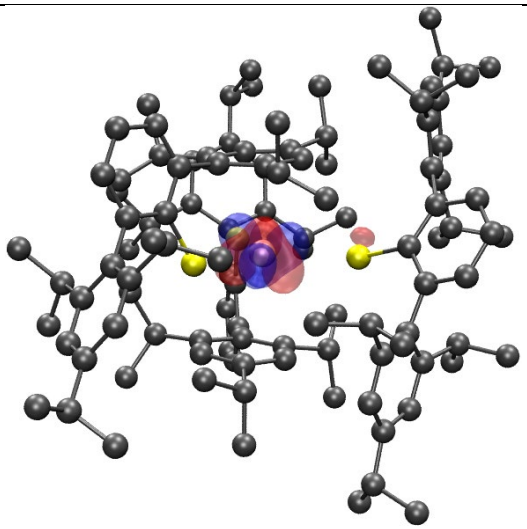	-3.083

HOMO (α)	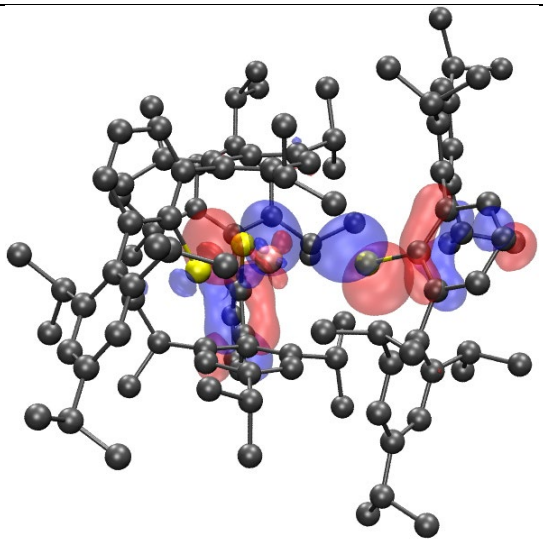	-5.010
HOMO-1 (α)	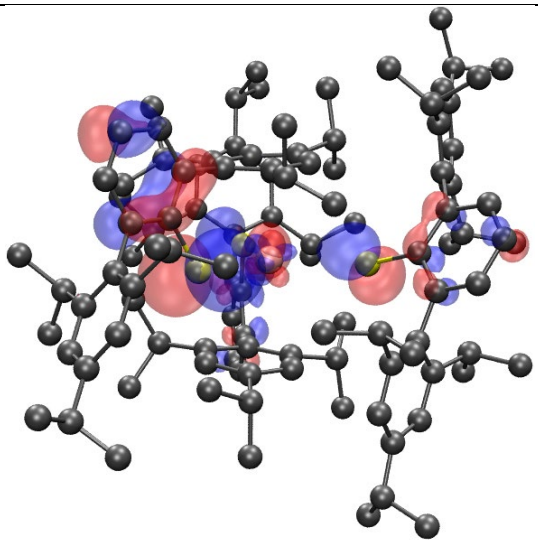	-5.138
HOMO-2 (α)	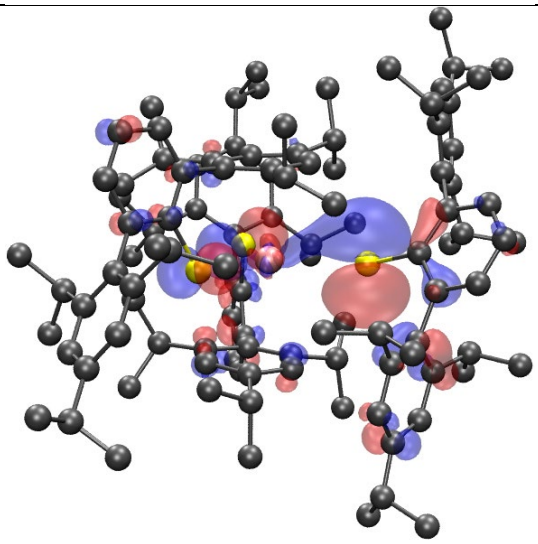	-5.223

The total (binding) energy and dispersion interaction were calculated from the geometry optimized structures and corrected for BSSE, which is tabulated in **Table S11** for both **3-La** and **3-Nd**.

Table S11. Binding energy, dispersion interaction energy and BSSE from DFT-d4 correction for La(SAr^{iPr6})$_3$, **3-La**, and Nd(SAr^{iPr6})$_3$, **3-Nd**, between the metal and ligand fragments and the ratios between each. The ratio of dispersion energy to binding energy accounts for BSSE.

	3-La	**3-Nd**
E_{bind} (kcal/mol)	-89.39	-96.54
E_{disp} (kcal/mol)	-48.06	-48.32
BSSE (kcal/mol)	-14.26	-13.95
E_{disp}/E_{bind}	0.4695	0.4372
E_{bind}/BSSE	0.1596	0.1445
E_{disp}/BSSE	0.2931	0.2888

Calculations of binding and dispersion energy were also performed for fragments consisting of the individual flanking ligands and the remaining structure containing the metal. These fragments will be referred to as “top” and “bottom” in reference to the flanking ligand chosen as a fragment. “Top” corresponds to the ligand containing S2 and “bottom” the ligand containing S3 from **Figures 3** and **4**. The results are summarized in **Table S12**. Note that some BSSEs are positive.

Table S12. Binding energy, dispersion interaction energy and BSSE from DFT-d4 correction for La(SAr^{iPr6})$_3$, **3-La**, and Nd(SAr^{iPr6})$_3$, **3-Nd**, between corresponding fragments and the ratios between each. The ratio of dispersion energy to binding energy accounts for BSSE.

	3-La		**3-Nd**	
	Top	**Bottom**	**Top**	**Bottom**
E_{bind} (kcal/mol)	-96.19	-90.81	-83.43	-85.50
E_{disp} (kcal/mol)	-48.33	-48.34	-47.93	-48.05
BSSE (kcal/mol)	-16.70	-15.11	-18.27	-15.15
E_{disp}/E_{bind}	0.4281	0.4564	0.4713	0.4774
E_{bind}/BSSE	0.1736	0.1664	0.2190	0.1772
E_{disp}/BSSE	0.3455	0.3125	0.3812	0.3153

Discussion. **3-La** and its constituent fragments are singlets in the ground state with no triplet or singlet instabilities. From **Table S7**, the geometry optimized structure of the full complex shows decent agreement with the X-ray structure. However, one of the flanking ligands is farther from the La atom in the optimized structure than in the X-ray structure as indicated by the increased distance from the corresponding sulfur and arene to the metal center.

3-Nd and the metal fragment are quartets in the ground state as **Table S8** shows that the doublet state yields structures higher in energy. The ligand fragment is a singlet in the ground state with no triplet or singlet instability. From **Table S9**, the geometry optimized structure of the full complex shows some agreement with the X-ray structure (for both spin states). The metal-sulfur bond distances are preserved, but the flanking arenes are significantly closer to the metal center. However, the centroid distances being different is preserved.

From **Table S11**, the energy contribution from dispersion is over half of the binding energy when corrected for BSSE for **3-La**. BSSE corrects for the overlapping basis sets between fragments

which would otherwise lead to overestimation of long-range effects.[13] Discussion of BSSEs will refer to their absolute values to be more intuitive. Despite the correction, dispersion accounts for a significant portion of the binding energy, indicating that dispersion is a major factor in interaction between the two fragments of **3-La**. However, the BSSE is moderate in comparison to the computed energies at about 16% of the binding energy and 29% of dispersion, leading to some uncertainty in the exact values.

For comparison, the dissociation reactions of the flanking ligands of **3-La** were also considered. Dispersion accounts for a similar portion of the binding energy compared to the case of the terminal ligand as shown in **Table S12**, with the top case having a slightly lower contribution from dispersion and the bottom case a slightly higher contribution. The BSSEs for the dissociations of both flanking ligands were marginally greater than the BSSE for the dissociation of the terminal ligand, so these values are slightly less certain than in the terminal ligand case.

Dispersion seems to contribute less to the binding energy in **3-Nd**. However, unlike **3-La**, these values are marginally more certain due to the lower BSSE, where it is a slightly smaller proportion of the binding energy and the dispersion energy in value. Regardless, dispersion still clearly accounts for a significant portion of the binding energy.

As for the flanking ligands of **3-Nd** as seen in **Table S6**, the bottom case yielded a similar BSSE to the flanking ligands of **3-La**, but the top case had the greatest BSSE out of any other case. Additionally, just as in **3-La**, the BSSEs of the flanking ligands are still slightly larger in comparison

to the terminal ligand case of **3-Nd**. Despite this, unlike **3-La**, both flanking ligand cases of **3-Nd** indicate that dispersion could potentially have a slightly greater contribution to the binding energy with the flanking ligands than in the terminal case.

7. Details of Construction of Quartz Furnace for the Synthesis of LnI_3.

We recently reported a procedure to synthesize large quantities (ca. 70 g) of unsolvated lanthanide triiodides involving the solid-state reactions between lanthanide metals (Ln) and ammonium iodide.[2] This method involves the use of a large tube furnace (Thermo Scientific Lindberg Blue M) that was 0.9 x 0.4 x 0.4 meters. This furnace did not fit in a typical 1.2 m fume hood and was therefore located on a bench adjacent to the hood with vacuum connections running to the inside of the hood. We now have constructed a smaller quartz furnace that permits the large-scale LnI_3 synthesis to be performed inside of a typical 1.2 m fume hood. The design of this furnace was based on one built by Jorg Meyer of the UC Irvine Glass Shop and described in a protocol that we previously published for the synthesis of NdI_2 and DyI_2.[28] Since that report did not describe the details of the furnace construction, the details of the construction of this new furnace and those of a new reaction apparatus are disclosed herein.

A quartz tube of dimensions 115 mm O.D. x 102 mm I.D. x 6.5 mm thickness was cut to a length of 160 mm at the UCI Glass Shop. To provide a means of securing the heating element, two 2 mm slots were cut into the top of the tube and two 2 mm slots were cut into the bottom of the tube. As shown in Figure S28, nichrome ribbon was then set into the top two slots in the tube and the quartz tube was then wrapped with 14 turns of the ribbon such that the wire was not in contact with itself at any point along the tube. The nichrome ribbon was then secured by setting the ribbon into the bottom two slots in the tube. Excess nichrome ribbon was left on the ends to be cut to an appropriate length after construction of the furnace was completed.

Figure S28. Image of the quartz tube that is used in the LnI_3 furnace showing the nichrome ribbon wrapped about its exterior. Note the slots that have been cut in the top and the bottom of the tube to secure the nichrome ribbon.

The nichrome ribbon will elongate when heated and this will result in the ribbon falling off the surface of the quartz tube and making contacts between the turns. To prevent this, the entire exterior of the quartz tube was coated with Rutland furnace cement (rated to be used up to 1090 °C), Figure S29. The tube was then baked at 120 °C for 1 h.

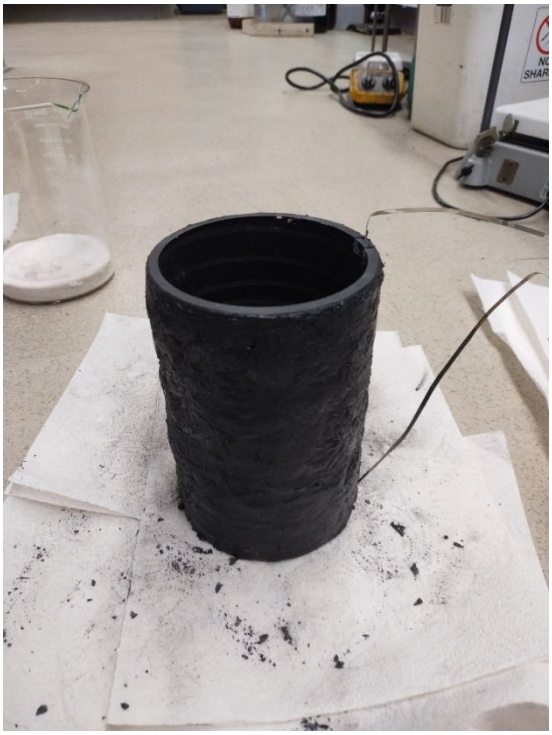

Figure S29. Image of the quartz tube after coating with furnace cement.

The quartz tube was then wrapped in a layer of 1/2" thick ceramic fiber mat (1" thick mat, purchased from Cedolio, and split in half) and the lower end of the nichrome wire was routed to the top of the tube along the outside of the ceramic fiber mat. The interior of a 2 L Pyrex borosilicate beaker was then coated in furnace cement. A 13 mm thick piece of ceramic mat was then cut into a circle of appropriate diameter to completely cover the bottom of the beaker. This ceramic mat was then placed in the bottom of the beaker and the quartz tube wrapped in ceramic fiber mat as described above was slid into the beaker such that both ends of the nichrome ribbon exit at the top of the beaker. The top of the beaker and quartz tube were then covered in a layer

of furnace cement. A 5 mm hole was made in the wet furnace cement at the top of the beaker so that gas could not become trapped in the space between the quartz tube and the inner wall of the beaker. The apparatus was then baked at 120 °C for 1 h, Figure S30.

Figure S30. Image of the furnace assembly after setting the quartz tube into the 2 L beaker and coating the top with furnace cement.

After baking the furnace assembly, the entire exterior of the beaker was coated in furnace cement. The exterior of the beaker was then wrapped in a layer of Zetek braided fiberglass tape, and the tape was coated with a thick layer of furnace cement. This step was taken to improve the structural integrity of the case of the furnace that is necessary at the high temperatures at which it is used. The apparatus was again baked at 120 °C for 1 h. Figure S31 shows the completed furnace.

Figure S31. Image of the completed furnace. The interior of the furnace has been filled with a layer of fiberglass wool to fill the void space between the reaction apparatus and the inner wall of the furnace.

The reaction apparatus, Figure S32, was assembled by modifying a large Chemglass sublimation apparatus (part number CG-3038-01). The bottom portion of the commercial apparatus was cut approximately 5 cm from the top of the lower part of the assembly and replaced with a longer, heavy-walled borosilicate tube at the UCI Glass Shop.

Figure S32. Images of the disassembled (top) and assembled (bottom) modified sublimation apparatus.

The assembled furnace and reaction vessel are shown in Figure S33. The LnI_3 synthesis can be carried out as previously described:[2] Ln metal pieces are combined with 10 equiv of ammonium iodide in the sublimation apparatus and the mixture is brought to a temperature of 375 °C over 10 min. The mixture is held at this temperature for 18 h. Then the apparatus is allowed to cool to ambient temperature and evacuated to 10^{-3} torr. The apparatus is then brought

to 430 °C over 10 min and held at this temperature for 3 h during which time the ammonium iodide was sublimed into the upper part of the sublimation apparatus. The apparatus is then allowed to cool to ambient temperature and sealed under reduced pressure. The apparatus is moved into a glovebox under argon atmosphere and the LnI_3 which remains in the bottom of the sublimation apparatus is collected.

The temperature of the furnace is controlled using a variable voltage regulator which is connected to the two ends of the nichrome ribbon by alligator clips as shown. The temperature is monitored using a digital thermometer equipped with a K-type thermocouple. Care must be

taken not to heat the apparatus too rapidly, as this can result in thermal strain in the borosilicate glass reaction vessel and ultimately to its failure.

Figure S33. Image of the furnace and sublimation apparatus assembled as used. When in operation, the glass tube at the top of the apparatus is connected to a Schlenk line in order to conduct the reaction under inert atmosphere. A digital thermometer equipped with a K-type thermocouple, which is used to monitor the temperature of the furnace, is shown at the bottom of the image, while the variable voltage regulator that supplies power to the furnace is shown to the left of the image. Alligator clips connecting the voltage regulator to the nichrome ribbon leads are shown at the right of the furnace.

The use of this smaller furnace allows the donor-free lanthanide triiodides to be synthesized at large scale in a fume hood. Another major advantage is that the bespoke borosilicate sublimation apparatus that was used in our previous method[2] for a large scale LnI_3 synthesis had to be broken and reassembled with each use. Using the modified sublimation apparatus described here, the large scale LnI_3 synthesis may be performed repeatedly without repair of the apparatus between syntheses. Additionally, this design permits the manipulation of the material at ambient temperature inside of a glovebox. Thus, infrared spectroscopy of the material may be collected on samples of the LnI_3 to assess the progress of the reaction, and additional heating of the material may be carried out, if necessary, without the need for breaking the sublimation apparatus and moving the material to new glassware.

8. References.

(1) Pangborn, A. B.; Giardello, M. A.; Grubbs, R. H.; Rosen, R. K.; Timmers, F. J. Safe and Convenient Procedure for Solvent Purification. *Organometallics* **1996**, *15* (5), 1518-1520.

(2) Stennett, C. R.; Luevano, M. R.; Queen, J. D.; Nguyen, J. Q.; Moore, W. N. G.; Evans, W. J. Large- and Small-Scale Syntheses of Donor-Free Rare-Earth Triiodides from the Metals and Ammonium Iodide. *Inorg. Chem.* **2024**, *63* (36), 16855-16860.

(3) Niemeyer, M.; Power, P. P. Donor-Free Alkali Metal Thiolates: Synthesis and Structure of Dimeric, Trimeric, and Tetrameric Complexes with Sterically Encumbered Terphenyl Substituents. *Inorg. Chem.* **1996**, *35* (25), 7264-7272.

(4) Gilbert-Bass, K.; Stennett, C. R.; Grotjahn, R.; Ziller, J. W.; Furche, F.; Evans, W. J. Exploring sulfur donor atom coordination chemistry with La(II), Nd(II), and Tm(II) using a terphenylthiolate ligand. *Chem. Commun.* **2024**, *60*, 4601-4604.

(5) APEX5 Version 2023.9-2. Bruker AXS, Inc.; Madison, WI: 2023.

(6) SAINT Version 8.40b. Bruker AXS, Inc.; Madison, WI: 2013.

(7) Sheldrick, G. M. SADABS, Version 2016/2. Bruker AXS, Inc.; Madison, WI: 2016.

(8) Sheldrick, G. M. SHELXTL, Version 2014/7. Bruker AXS Inc.; Madison WI: 2014.

(9) *International Tables for Crystallography, Vol. C*; Dordrecht: Kluwer Academic Publishers, 1992.

(10) APEX2 Version 2014.11-0. Bruker AXS Inc.; Madison WI: 2014.

(11) Sheldrick, G. M. SADABS, Version 2014/5. Bruker AXS Inc.; Madison WI: 2014.

(12) APEX4 Version 2021.4-0. Bruker AXS Inc.; Madison WI: 2021.

(13) Spek, A. L. *PLATON SQUEEZE*: a tool for the calculation of the disordered solvent contribution to the calculated structure factors. *Acta Crystallographica Section C* **2015**, *71* (1), 9-18.

(14) Spek, A. L. Structure validation in chemical crystallography. *Acta Crystallographica Section D* **2009**, *65* (2), 148-155.

(15) Franzke, Y. J.; Holzer, C.; Andersen, J. H.; Begušić, T.; Bruder, F.; Coriani, S.; Della Sala, F.; Fabiano, E.; Fedotov, D. A.; Fürst, S.; et al. TURBOMOLE: Today and Tomorrow. *Journal of Chemical Theory and Computation* **2023**, *19* (20), 6859-6890.

(16) Eichkorn, K.; Treutler, O.; Öhm, H.; Häser, M.; Ahlrichs, R. Auxiliary basis sets to approximate Coulomb potentials. *Chem. Phys. Lett.* **1995**, *240* (4), 283-289.

(17) Klamt, A.; Schüürmann, G. COSMO: a new approach to dielectric screening in solvents with explicit expressions for the screening energy and its gradient. *J. Chem. Soc. Perkin Trans. 2* **1993**, (5), 799-805.

(18) Schäfer, A.; Horn, H.; Ahlrichs, R. Fully optimized contracted Gaussian basis sets for atoms Li to Kr. *J. Chem. Phys.* **1992**, *97* (4), 2571-2577.

(19) Weigend, F.; Ahlrichs, R. Balanced basis sets of split valence, triple zeta valence and quadruple zeta valence quality for H to Rn: Design and assessment of accuracy. *Physical Chemistry Chemical Physics* **2005**, *7* (18), 3297-3305.

(20) Dolg, M.; Stoll, H.; Preuss, H. Energy-adjusted ab initio pseudopotentials for the rare earth elements. *J. Chem. Phys.* **1989**, *90* (3), 1730-1734.

(21) Staroverov, V. N.; Scuseria, G. E.; Tao, J.; Perdew, J. P. Comparative assessment of a new nonempirical density functional: Molecules and hydrogen-bonded complexes. *J. Chem. Phys.* **2003**, *119* (23), 12129-12137.

(22) Caldeweyher, E.; Ehlert, S.; Hansen, A.; Neugebauer, H.; Spicher, S.; Bannwarth, C.; Grimme, S. A generally applicable atomic-charge dependent London dispersion correction. *J. Chem. Phys.* **2019**, *150* (15), 154122.

(23) Bauernschmitt, R.; Ahlrichs, R. Stability analysis for solutions of the closed shell Kohn–Sham equation. *J. Chem. Phys.* **1996**, *104* (22), 9047-9052.

(24) Treutler, O.; Ahlrichs, R. Efficient molecular numerical integration schemes. *J. Chem. Phys.* **1995**, *102* (1), 346-354.

(25) Deglmann, P.; May, K.; Furche, F.; Ahlrichs, R. Nuclear second analytical derivative calculations using auxiliary basis set expansions. *Chem. Phys. Lett.* **2004**, *384* (1), 103-107.

(26) Humphrey, W.; Dalke, A.; Schulten, K. VMD: Visual molecular dynamics. *J. Molec. Graphics* **1996**, *14* (1), 33-38.

(27) Boys, S. F.; Bernardi, F. The calculation of small molecular interactions by the differences of separate total energies. Some procedures with reduced errors. *Mol. Phys.* **1970**, *19* (4), 553-566.

(28) Evans, W. J.; Allen, N. T.; Workman, P. S.; Meyer, J. C. Large Scale Synthesis of Dysprosium and Neodymium Diiodides. *Inorg. Chem.* **2003**, *42* (9), 3097--3099.